



CMS-HIG-19-002

CERN-EP-2020-106
2021/03/10

Measurement of the inclusive and differential Higgs boson production cross sections in the leptonic WW decay mode at $\sqrt{s} = 13$ TeV

The CMS Collaboration*

Abstract

Measurements of the fiducial inclusive and differential production cross sections of the Higgs boson in proton-proton collisions at $\sqrt{s} = 13$ TeV are performed using events where the Higgs boson decays into a pair of W bosons that subsequently decay into a final state with an electron, a muon, and a pair of neutrinos. The analysis is based on data collected with the CMS detector at the LHC during 2016–2018, corresponding to an integrated luminosity of 137 fb^{-1} . Production cross sections are measured as a function of the transverse momentum of the Higgs boson and the associated jet multiplicity. The Higgs boson signal is extracted and simultaneously unfolded to correct for selection efficiency and resolution effects using maximum-likelihood fits to the observed distributions in data. The integrated fiducial cross section is measured to be $86.5 \pm 9.5\text{ fb}$, consistent with the Standard Model expectation of $82.5 \pm 4.2\text{ fb}$. No significant deviation from the Standard Model expectations is observed in the differential measurements.

"Published in the Journal of High Energy Physics as doi:10.1007/JHEP03(2021)003."

1 Introduction

The Higgs boson, observed by the ATLAS and CMS experiments [1–3], has a rich set of properties whose measurements will have a significant impact on the understanding of the physics of the standard model (SM) and possible extensions beyond the SM (BSM). Extensive effort has been dedicated to determine its quantum numbers and couplings with ever-improving accuracy due to the large data sample delivered by the CERN LHC and innovations in analysis techniques.

The differential production cross sections of the Higgs boson can be predicted with high precision and can therefore provide a useful probe of the effects from higher-order corrections in perturbative theory or any deviation of its properties from the SM expectations. In particular, the differential cross section as a function of the transverse momentum of the Higgs boson (p_T^H) is computed up to next-to-next-to-leading order (NNLO) in quantum chromodynamics (QCD) [4–9], and is known to be sensitive to possible deviations from the SM in the Yukawa couplings of light quarks [10] and to effective operators of dimension six or higher in BSM Lagrangians [11].

We present measurements of differential cross sections for Higgs boson production in proton-proton (pp) collisions at $\sqrt{s} = 13$ TeV within a fiducial region, as a function of p_T^H and jet multiplicity (N_{jet}). These two observables are collectively referred to as differential-basis observables (\mathcal{DO}) hereafter. The measurements include all Higgs boson production modes. Higgs bosons decaying to two W bosons that subsequently decay leptonically into the $e^\pm \mu^\mp \nu \bar{\nu}$ final state are considered. The data in these measurements were recorded at the CMS experiment and correspond to an integrated luminosity of 137 fb^{-1} .

Inclusive Higgs boson production cross sections in the $H \rightarrow W^+W^-$ decay mode have been performed by both ATLAS and CMS [12, 13] at $\sqrt{s} = 13$ TeV with smaller data samples. Both experiments have also reported measurements of differential production cross sections of the Higgs boson with smaller data samples [14, 15]. In particular, the CMS Collaboration has measured cross sections as a function of several observables, including p_T^H and N_{jet} , using Higgs bosons decaying into pairs of photons [16] and Z bosons [17] at $\sqrt{s} = 13$ TeV in 35.9 fb^{-1} of data. These measurements have been combined [15], including in the p_T^H spectra data from the search for the Higgs boson produced with large p_T and decaying to a bottom quark-antiquark pair [18]. The larger branching ratio makes the $e^\pm \mu^\mp \nu \bar{\nu}$ final state competitive with the two-photon and two-Z boson channels. Additionally, unlike the decay channel into a bottom quark-antiquark pair, identification of Higgs boson production events in the $e^\pm \mu^\mp \nu \bar{\nu}$ final state does not require the Higgs boson to be boosted, allowing the full range of p_T^H to be studied. In the $H \rightarrow W^+W^-$ channel, previous measurements of the differential cross sections were reported in data collected at $\sqrt{s} = 8$ TeV [19, 20]. Measurements reported in this paper have been performed for the first time in the $H \rightarrow W^+W^-$ decay channel at $\sqrt{s} = 13$ TeV, exploiting the full data sample available. The methods for the determination of the differential cross section have been updated substantially compared to the 8 TeV measurement [20], combining the signal extraction, unfolding, and regularization into a single simultaneous fit.

2 The CMS detector and object selection

The central feature of the CMS apparatus is a superconducting solenoid of 6 m internal diameter, providing a magnetic field of 3.8 T. Within the solenoid volume are a silicon pixel and strip tracker, a lead tungstate crystal electromagnetic calorimeter (ECAL), and a brass and scin-

tillator hadron calorimeter (HCAL), each composed of a barrel and two endcap sections. Forward calorimeters extend the pseudorapidity (η) coverage provided by the barrel and endcap detectors. Muons are detected using three technologies: drift tubes, cathode strip chambers, and resistive-plate chambers embedded in the steel flux-return yoke outside the solenoid. The muon detectors cover the full 2π of azimuth (ϕ) about the beam axis and a range of $|\eta| < 2.4$.

Events of interest are selected using a two-tiered trigger system [21]. The first level (L1), composed of specialized hardware processors, uses information from the calorimeters and muon detectors to select events at a rate of ≈ 100 kHz within a fixed time interval of $4\ \mu\text{s}$. The second level, known as the high-level trigger (HLT), consists of a farm of processors running a version of the full event reconstruction software optimized for fast processing, and reduces the event rate to ≈ 1 kHz before data storage.

A more detailed description of the CMS detector, together with a definition of the coordinate system and the kinematic variables, can be found in Ref. [22].

Electrons are identified and their momentum measured in the pseudorapidity interval $|\eta| < 2.5$ by combining the energy measurement in the ECAL, the momentum measurement in the tracker and the energy sum of all bremsstrahlung photons spatially compatible with originating from the electron track. The single electron trigger efficiency exceeds 90% over the full η range, the efficiency to reconstruct and identify electrons ranges between 60 and 80% depending on the lepton p_{T} . The momentum resolution for electrons with $p_{\text{T}} \approx 45$ GeV from $Z \rightarrow ee$ decays ranges from 1.7 to 4.5% depending on the η region. The resolution is generally better in the barrel than in the endcaps and also depends on the bremsstrahlung energy emitted by the electron as it traverses the material in front of the ECAL [23].

Muons are identified and their momentum measured in the pseudorapidity interval $|\eta| < 2.4$ matching tracks in the muon chambers and in the silicon tracker. The single muon trigger efficiency exceeds 90% over the full η range, and the efficiency to reconstruct and identify muons is greater than 96%. The relative transverse momentum resolution for muons with p_{T} up to 100 GeV is 1% in the barrel and 3% in the endcaps [24, 25].

Proton-proton interaction vertices are reconstructed from tracks using the Adaptive Vertex Fitting algorithm [26]. The candidate vertex with the largest value of summed physics-object p_{T}^2 is taken to be the primary pp interaction vertex. The physics objects are the track-only jets, clustered using the jet finding algorithm [27, 28] with the tracks assigned to candidate vertices as inputs, and the associated missing transverse momentum, taken as the negative vector sum of the p_{T} of those jets.

The particle-flow (PF) algorithm [29] aims to reconstruct and identify each individual particle in an event, with an optimized combination of information from the various elements of the CMS detector. The momenta of electrons and muons are obtained as described above. The energies of photons are based on the measurement in the ECAL. The energies of charged hadrons are determined from a combination of their momenta measured in the tracker and the matching ECAL and HCAL energy deposits. Finally, the energies of neutral hadrons are obtained from their corresponding corrected ECAL and HCAL energies. Such reconstructed particle candidates are generically referred to as PF candidates.

The hadronic jets in each event are clustered from the PF candidates using the anti- k_{T} algorithm [27, 28] with a distance parameter of 0.4. The jet momentum is determined from the vectorial sum of all particle momenta in the jet. From simulation, reconstructed jet momentum is found to be, on average, within 5 to 10% of the momentum of generator jets, which are jets clustered from all generator final-state particles excluding neutrinos, over the entire p_{T} spec-

trum and detector acceptance. Additional pp interactions within the same or nearby bunch crossings (pileup) can contribute additional tracks and calorimetric energy deposits to the jet momentum. To mitigate this effect, charged particles identified as originating from pileup vertices are discarded and an offset correction is applied to correct for remaining contributions from neutral pileup particles [29]. Jet energy corrections are derived from simulation studies so that the average measured response of jets becomes identical to that of generator jets. In situ measurements of the momentum imbalance in dijet, photon + jet, Z + jet, and multijet events are used to account for any residual differences in jet energy scale in data and simulation [30, 31]. The jet energy resolution amounts typically to 15% at 10 GeV, 8% at 100 GeV, and 4% at 1 TeV. Additional selection criteria are applied to each jet to remove jets potentially dominated by anomalous contributions from various subdetector components or reconstruction failures. Jets are measured in the range $|\eta| < 4.7$. In the analysis of data recorded in 2017, to eliminate spurious jets caused by detector noise, all jets were excluded in the range $2.5 < |\eta| < 3.0$.

The identification of jets containing hadrons with bottom quarks is referred to as b tagging. For each reconstructed jet, a b tagging score is calculated through a multivariate analysis of jet properties based on a boosted decision tree algorithm and deep neural networks [32]. Jets are considered b tagged if this score is above a threshold set to achieve $\approx 80\%$ efficiency for bottom-quark jets in $t\bar{t}$ events. For this threshold, the probability of misidentifying charm-quark and light-flavor jets produced in $t\bar{t}$ events as bottom-quark jets is $\approx 6\%$.

Missing transverse momentum (\vec{p}_T^{miss}) is defined as the negative vector sum of the transverse momenta of all the PF candidates in an event [33], weighted by their estimated probability to originate from the primary interaction vertex. The pileup-per-particle identification algorithm [34] is employed to calculate this probability.

3 Data sets and simulated samples

The analyzed data sets were recorded in 2016, 2017, and 2018, with corresponding integrated luminosities of 35.9, 41.5, and 59.7 fb^{-1} , respectively [35–37].

The events in this analysis are selected through HLT algorithms that require the presence of either a single high- p_T lepton or both an electron and a muon at lower p_T thresholds that pass identification and isolation requirements. The requirements in the single-lepton triggers are more restrictive than in the electron-muon triggers, but are less stringent than those applied in the event-selection stage. In the 2016 data set, the p_T threshold of the single-electron trigger is 25 GeV for $|\eta| < 2.1$ and 27 GeV for $2.1 < |\eta| < 2.5$, although the use of tight L1 p_T constraints at the beginning of the fill made the effective thresholds higher. The threshold for the single-muon trigger is 24 GeV for $|\eta| < 2.4$. The p_T thresholds in the dilepton trigger are respectively 23 and 8 GeV for the leading and trailing (second highest p_T) leptons for the first part of the data set corresponding to an integrated luminosity of 17.7 fb^{-1} . The threshold for the trailing lepton is raised to 12 GeV in the later part of the 2016 data set. In the 2017 data set, single-electron and single-muon p_T thresholds are raised to 35 and 27 GeV, respectively. The corresponding thresholds in the 2018 data set are 32 and 24 GeV. The dilepton triggers in the 2017 and 2018 data sets have the same thresholds as given above for the latter part of the 2016 data set.

Monte Carlo (MC) simulated events are used in this analysis for signal modeling and background estimation. To account for changes in detector and pileup conditions and to incorporate the latest updates of the reconstruction software, a different simulation is used in the analysis of each of the 2016, 2017, and 2018 data sets. Different event generators are used de-

pending on the simulated hard scattering processes, but parton distribution functions (PDFs) and underlying event (UE) tunes are common to all simulated events for a given data set. The parton-showering and hadronization processes are simulated through PYTHIA [38] 8.226 (8.230) in 2016 (2017 and 2018). The PDF set is NNPDF 3.0 [39, 40] (3.1 [41]) and the UE tune is CUETP8M1 [42] (CP5 [43]) for the 2016 sample (2017 and 2018 samples).

Higgs boson production through gluon-gluon fusion (ggF), vector-boson fusion (VBF), weak-boson associated production (VH, with V representing either the W or Z boson), and tt} associated production (tt}H), are considered as signal processes in this analysis. Weak boson associated production has contributions from quark- and gluon-induced Z boson associated production and W boson associated production. Events for all signal production channels are generated using POWHEG v2 [44–50] at next-to-leading order (NLO) accuracy in QCD, including finite quark mass effects. The ggF events are further reweighted to match the NNLOPS [6, 7] prediction in the distributions of p_T^H and N_{jet} . The reweighting is based on p_T^H and N_{jet} as computed in the Higgs boson simplified template cross section (STXS) scheme 1.0 [51]. All signal samples are normalized to the cross sections recommended in [52]. In particular, the ggF sample is normalized to next-to-next-to-next-to-leading order (N3LO) QCD accuracy and NLO electroweak accuracy [53–55]. Alternative sets of events for ggF and VBF production using the MADGRAPH5_aMC@NLO v2.2.2 generator [56] are used for comparison with the extracted differential cross sections. The alternative ggF sample is generated with up to two extra partons merged through the FxFx scheme [57] in the infinite top quark mass limit. The Higgs boson mass is assumed to be 125 GeV for these simulations.

The JHUGEN generator [58] (v5.2.5 and 7.1.4 in 2016 and 2017–2018, respectively) is used to simulate the decay of the Higgs boson into two W bosons and subsequently into leptons for the VBF events in 2016, ggF and VBF events from 2017 and 2018, and quark-induced ZH production in 2017 and 2018. The decay of the Higgs boson in other signal samples is simulated through PYTHIA 8.212 along with the parton shower (PS) and hadronization. Higgs boson that decays into a $\tau^+\tau^-$ pair is considered as background in this analysis.

Quark-initiated nonresonant W boson pair production (W^+W^-) is simulated at NLO with POWHEG v2 [59]. Gluon-initiated, loop-induced nonresonant W^+W^- is simulated with MCFM v7.0 [60–62] and normalized to its NLO cross section [63]. The tt} and single top production (tt} + tW) are simulated with POWHEG v2 [64–66]. The Drell–Yan τ lepton pair production ($\tau^+\tau^-$) is simulated with MADGRAPH5_aMC@NLO v2.4.2 with up to two additional jets at NLO accuracy. Radiative W production ($W\gamma$) is simulated with MADGRAPH5_aMC@NLO v2.4.2 with up to 3 additional jets at LO accuracy. Other diboson processes involving at least one Z boson or a virtual photon (γ^*) with mass down to 100 MeV are simulated with POWHEG v2 [59]. Associated $W\gamma^*$ production with virtual photon mass below 100 MeV is simulated by the parton shower on top of the $W\gamma$ sample. The $W\gamma^*$ prediction is corrected with a scale factor extracted from a trilepton control region, following the approach described in Ref. [13]. Purely electroweak W^+W^- plus two jets production is simulated at LO with MADGRAPH5_aMC@NLO v2.4.2. Multiboson production with more than two vector bosons is simulated at NLO with MADGRAPH5_aMC@NLO v2.4.2.

The simulated quark-induced W^+W^- background is weighted event-by-event to match the transverse momentum distribution of the W^+W^- system to NNLO plus next-to-next-to leading logarithm (NNLL) accuracy in QCD [67, 68]. It is also weighted to include the effect of electroweak corrections, computed based on Ref. [69]. The tt} component of the tt} + tW background and the $\tau^+\tau^-$ events are also weighted to improve agreement of the simulated p_T distributions of the tt} and Drell–Yan systems with data [70, 71].

For all processes, the detector response is simulated using a detailed description of the CMS detector, based on the GEANT4 package [72]. To model multiple pp collisions in one beam crossing, minimum bias events simulated in PYTHIA are overlaid onto each event, with the number of interactions drawn from a distribution that is similar to the observed distribution. The average number of such interactions per event is ≈ 23 for the 2016 data, and 32 for the 2017 and 2018 data.

To mitigate the discrepancies between data and simulation in various distributions, simulated events are reweighted according to relevant lepton or jet kinematic variables. Discrepancies due to multiple causes, such as the difference in the pileup distribution and the imperfect modeling of the detector, are corrected using weights derived from comparisons of simulation with observed data in control regions.

4 Analysis strategy

The differential production cross sections are measured using dilepton event samples selected based on the reconstructed properties of the leptons and \vec{p}_T^{miss} . Events passing the selections described in Section 5 are referred to as signal candidate events, and are split into reconstruction-level (\mathcal{RL}) bins of the \mathcal{DO} . The $\mathcal{RL} p_T^H$ is computed as the magnitude of the vectorial sum of the transverse momenta of the two lepton candidates and \vec{p}_T^{miss} . The missing transverse momentum represents the total vector p_T of the two neutrinos that escape detection. The $\mathcal{RL} N_{\text{jet}}$ is the number of jets with $p_T > 30 \text{ GeV}$ and $|\eta| < 4.7$.

The signal candidate events are dominated by background processes, with main contributions from W^+W^- , $t\bar{t} + tW$, $\tau^+\tau^-$, and events with misidentified leptons or leptons from heavy-flavor hadron decays (nonprompt leptons). The total number of signal events in the sample is extracted by template fitting techniques, exploiting quantities that separate signal and background.

Two observables, the dilepton mass (m^{ll}) and the transverse mass of the Higgs boson (m_T^H), are found to have strong discrimination power against background processes. The value of m_T^H can be defined as

$$m_T^H = \sqrt{2p_T^{ll}p_T^{\text{miss}}[1 - \cos \Delta\phi(\vec{p}_T^{ll}, \vec{p}_T^{\text{miss}})]}, \quad (1)$$

where p_T^{ll} is the magnitude of the vector sum of the transverse momenta of the two lepton candidates, and $\Delta\phi(\vec{p}_T^{ll}, \vec{p}_T^{\text{miss}})$ is the azimuthal angle between \vec{p}_T^{ll} and \vec{p}_T^{miss} .

Signal candidate events in individual \mathcal{RL} bins are therefore sorted into two-dimensional (m^{ll}, m_T^H) histograms. The number of Higgs boson production signal events in each histogram can be inferred by fitting it with a model that consists of a sum of background and signal templates, obtained from their respective expected distributions. The estimation of the background is described briefly in Section 6 and more thoroughly in Refs. [13, 73]. Signal expectations are derived from the simulated event samples described in Section 3. There is only a small dependence of the signal (m^{ll}, m_T^H) shape on production mode, thus distributions from the four Higgs boson production modes are combined with their relative normalizations fixed to the SM predictions.

To extract differential cross section measurements from such fits, signal templates from different bins of \mathcal{DO} values predicted by the event generator (generator-level, \mathcal{GL} , bins) are individually assigned a priori unconstrained normalization factors. Initial normalizations of the signal templates are set to the SM expectations. The best fit normalization factor for the templates of a

\mathcal{GL} bin i can therefore be interpreted as its signal strength modifier $\mu_i = \sigma_i^{\text{obs}} / \sigma_i^{\text{SM}}$, where σ_i^{obs} and σ_i^{SM} are the observed and predicted fiducial cross sections in bin i .

Generator-level and \mathcal{RL} observable values are not perfectly aligned due to resolution and energy scale effects. For this reason, signal events from one \mathcal{GL} bin i contribute to multiple \mathcal{RL} bin templates, which are all scaled together by μ_i . Therefore, by performing one simultaneous fit over all \mathcal{RL} bin histograms, signal strength modifiers of the \mathcal{GL} observable bins can be determined exploiting the full statistical power of the data set. This fit extracts the signal and simultaneously unfolds the measured cross sections into the \mathcal{GL} bins, correctly propagating the experimental covariance matrix. The unfolding procedure can be highly sensitive to statistical fluctuations in the observed distributions, especially for the p_T^H measurement, where the contributions from each \mathcal{GL} bin into multiple \mathcal{RL} bins are significant. To mitigate this effect, a regularization procedure is introduced in the fit for the p_T^H measurement to obtain the final result. More details about the fiducial phase space, the fit, and the regularization scheme are given in Section 7.

5 Event selection

The selection of signal candidate events starts with a requirement of at least two charged lepton candidates, where the two with the highest p_T (leading and trailing lepton candidates) have tracks associated with the primary vertex, and have opposite charge. The two leptons must be an electron and a muon to suppress Drell–Yan background. Charged leptons are required to satisfy the isolation criterion that the scalar sum of the p_T of PF candidates associated with the primary vertex, exclusive of the lepton itself, and neutral PF particles in a cone of a radius $\Delta R = \sqrt{(\Delta\eta)^2 + (\Delta\phi)^2} = 0.4$ (0.3), where ϕ is the azimuthal angle in radians, centered on the muon (electron) direction is below a threshold of 15 (6)% relative to the muon (electron) p_T . To mitigate the effect of the pileup on this isolation variable, a correction based on the average energy density in the event [74] is applied. Additional requirements on the transverse and longitudinal impact parameters with respect to the primary vertex are included. An algorithm based on the evaluation of the track hits in the first tracker layers is used to reject electrons arising from photon conversions. The transverse momenta of the leading and trailing lepton candidates, $p_T^{l_1}$ and $p_T^{l_2}$, must be greater than 25 and 13 GeV, respectively, so that the electron-muon triggers are efficient. To ensure high reconstruction efficiencies, only electron candidates with $|\eta| < 2.5$ and muon candidates with $|\eta| < 2.4$ are considered. Other lepton candidates in the event, if there are any, must have $p_T < 10$ GeV.

Signal candidate events must further satisfy $p_T^{\text{miss}} > 20$ GeV and $p_T^{ll} > 30$ GeV to discriminate against QCD multijet and $\tau^+\tau^-$ backgrounds. The contribution from the $\tau^+\tau^-$ background, including that from the low-mass Drell–Yan process, is further suppressed by the requirements $m^{ll} > 12$ GeV, $m_T^H > 60$ GeV, and $m_T^{l_2} > 30$ GeV. Here the last quantity is defined by

$$m_T^{l_2} = \sqrt{2p_T^{l_2} p_T^{\text{miss}} \left[1 - \cos \Delta\phi(\vec{p}_T^{l_2}, \vec{p}_T^{\text{miss}}) \right]}, \quad (2)$$

where $\vec{p}_T^{l_2}$ is the transverse momentum of the trailing lepton, $p_T^{l_2}$ is the magnitude, and $\Delta\phi(\vec{p}_T^{l_2}, \vec{p}_T^{\text{miss}})$ is the opening azimuthal angle relative to \vec{p}_T^{miss} . This observable stands as a proxy to the mass of the virtual W boson from the Higgs boson decay. As such, the last criterion also limits the contribution from nonprompt lepton background due to single W boson production, when the trailing lepton candidate is a misidentified jet and therefore has little correlation with \vec{p}_T^{miss} .

Finally, to suppress $t\bar{t} + tW$ events, the events are required to have no b-tagged jets with $p_T > 20 \text{ GeV}$.

The event selection criteria are identical among the three data sets, aside from certain details such as the definition of b tagging. The efficiencies of the signal candidate selection for identifying ggF events with W bosons decaying to leptons are 2.8, 3.6, and 3.6% for the 2016, 2017, and 2018 data sets, respectively. The differences in efficiencies arise mainly from the requirements set on lepton identification and p_T^{miss} resolution.

Within each \mathcal{RL} bin of the \mathcal{DO} , signal candidate events are categorized by $p_T^{l_2}$ and flavors of the leptons to maximize the sensitivity to signal. Categories with $p_T^{l_2} < 20 \text{ GeV}$ receive, in comparison to those with $p_T^{l_2} > 20 \text{ GeV}$, more contributions from nonprompt-lepton background but less from W^+W^- and $t\bar{t}$ processes, and result in fewer total background events. However, the Higgs boson signal is expected to contribute evenly to the two $p_T^{l_2}$ regions, providing thereby categories with $p_T^{l_2} < 20 \text{ GeV}$ with larger signal-to-background ratios. Since nonprompt leptons are more likely to arise from jets misidentified as electrons, categorization within the two regions by the flavor of the leptons helps increase the sensitivity by creating two regions with a different signal-to-background ratio. This four-way categorization ($4\mathcal{W}$) is applied to reconstructed \mathcal{DO} bins with a sufficiently large expected number of events. For bins with fewer expected events, categorization is reduced to three-way ($3\mathcal{W}$, using $p_T^{l_2}$, and flavor categorization for $p_T^{l_2} < 20 \text{ GeV}$), two-way ($2\mathcal{W}$, using just $p_T^{l_2}$), or none ($1\mathcal{W}$). In the most sensitive categories, the ratio of expected signal yield to the expected total number of events is ≈ 0.08 , and the ratio of expected signal events to the square root of expected background events is 3.5.

Control regions for $t\bar{t} + tW$ and $\tau^+\tau^-$ background processes are used to constrain the estimates of these processes in the simultaneous fit. The definitions of the two control regions follow that of the signal region closely to make the event kinematics similar among the three regions. Specifically, both control regions share all event selection criteria with the signal region except for the requirements on m^{ll} , m_T^H , $m_T^{l_2}$, and the number of b-tagged jets. The $t\bar{t} + tW$ control region instead requires $m^{ll} > 50 \text{ GeV}$ and at least one b-tagged jet with $p_T > 20 \text{ GeV}$. If there is another jet in the event with $p_T > 30 \text{ GeV}$, the b-tagged jets must also have $p_T > 30 \text{ GeV}$. There is no constraint on m_T^H , and the requirement $m_T^{l_2} > 30 \text{ GeV}$ is common with the signal region. The $\tau^+\tau^-$ control region requires $40 < m^{ll} < 80 \text{ GeV}$ and $m_T^H < 60 \text{ GeV}$, and has no constraint on $m_T^{l_2}$. The restriction of having no b-tagged jets with $p_T > 20 \text{ GeV}$ is common with the signal region.

6 Background modeling

All background processes, except for that from nonprompt lepton events, are modeled using MC simulation. The nonprompt lepton background is modeled by applying weights to events containing lepton candidates passing less stringent selection criteria than those used in the signal region. These weights, called fake-lepton factors, are obtained from the probability of a jet being misidentified as a lepton and the efficiency of correctly reconstructing and identifying a lepton. More details about this method are given in Ref. [13]. The validity of this background estimate is checked by comparing the prediction of the (m^{ll}, m_T^H) distribution of the nonprompt lepton events to the observed distribution in a control region with two leptons of the same charge.

Different constraints are applied to the background template normalization, to reflect our knowl-

Table 1: Definition of the fiducial region.

Observable	Condition
Lepton origin	Direct decay of $H \rightarrow W^+W^-$
Lepton flavors; lepton charge	$e \mu$ (not from τ decay); opposite
Leading lepton p_T	$p_T^{l_1} > 25 \text{ GeV}$
Trailing lepton p_T	$p_T^{l_2} > 13 \text{ GeV}$
$ \eta $ of leptons	$ \eta < 2.5$
Dilepton mass	$m^{ll} > 12 \text{ GeV}$
p_T of the dilepton system	$p_T^{ll} > 30 \text{ GeV}$
Transverse mass using trailing lepton	$m_T^{l_2} > 30 \text{ GeV}$
Higgs boson transverse mass	$m_T^H > 60 \text{ GeV}$

edge of the cross section of those processes in the model. First, the normalizations of the templates of the three main background processes, i.e., W^+W^- , $t\bar{t} + tW$, and $\tau^+\tau^-$, are left unconstrained separately in each \mathcal{RL} bin. This treatment reflects the belief that precise predictions of these background processes are essential, but the MC simulation cannot be trusted at extreme values of the observables, especially large N_{jet} . Their normalizations are therefore determined from the observed data. To help constrain $t\bar{t} + tW$ and $\tau^+\tau^-$, control samples enriched in the two processes (see Section 5) are included in the simultaneous fit. The normalizations of the $t\bar{t} + tW$ and $\tau^+\tau^-$ templates in these control samples are fit with factors that also scale the respective templates in the fit to the signal candidate events. The normalization of the W^+W^- template is determined without using specific control samples, and is mostly constrained by the high m^{ll} region.

Normalizations of the templates for the minor background processes are centered at the SM expectations and are constrained a priori by their respective systematic uncertainties. Normalizations of the nonprompt lepton templates are centered at the estimates given by the method described above. Because the closure of the nonprompt background estimation method depends on the flavor composition of the jets faking the leptons, and since the flavor composition varies among \mathcal{DO} bins, the normalization of the nonprompt background is allowed to vary independently in each of those bins.

7 Definition of the fiducial region and extraction of the signal

The fiducial region is defined in Table 1, with all quantities evaluated at generator level after parton showering and hadronization. Leptons are “dressed”, i.e., momenta of photons radiated by leptons within a cone of $\Delta R = \sqrt{(\Delta\eta)^2 + (\Delta\phi)^2} < 0.1$ are added to the lepton momentum. The fiducial region definition matches that of the event selection criteria, except for the η bound of muons ($|\eta| < 2.4$ in the event selection) and the absence of any direct selection of p_T^{miss} . Generator level m_T^H and $m_T^{l_2}$ employ a generator level \vec{p}_T^{miss} definition corresponding to the vector sum of all neutrinos in the event. The expected fiducial cross section and its theoretical uncertainty [52] computed for the nominal signal is

$$\sigma^{\text{SM}} = 82.5 \pm 4.2 \text{ fb}, \quad (3)$$

This cross section is estimated using, for each process, the cross sections recommended in [52] and estimating the acceptance of the fiducial region from the nominal signal samples.

The differential production cross sections for the Higgs boson are inferred from the signal strength modifiers extracted through a simultaneous fit to all bins and categories of signal can-

dicate events and two control regions. The systematic uncertainties discussed in Section 8 are represented by constrained or unconstrained nuisance parameters that affect the shapes and normalizations of the signal and background templates. The simultaneous fit maximizes the likelihood function

$$\mathcal{L}(\boldsymbol{\mu}; \boldsymbol{\theta}) = \prod_j \text{Poisson}\left(n_j; s_j(\boldsymbol{\mu}; \boldsymbol{\theta}) + b_j(\boldsymbol{\theta})\right) \mathcal{N}(\boldsymbol{\theta}) \mathcal{K}(\boldsymbol{\mu}). \quad (4)$$

In the formula, $\boldsymbol{\mu}$ and $\boldsymbol{\theta}$ are vectors of the signal strength modifiers and nuisance parameters, respectively. The expression $\text{Poisson}(n; \lambda)$ represents the Poisson probability of observing n events when expecting λ , and n_j is the observed number of events in a given bin of the (m_T^H, m_T^H) template in any \mathcal{RL} category, with index j running over bins of histograms of signal region categories and control regions for all the \mathcal{RL} \mathcal{DO} bins, and all three data sets. The signal in the j th bin is represented by

$$s_j(\boldsymbol{\mu}; \boldsymbol{\theta}) = \sum_{i=1}^N \left[A_{ji}(\boldsymbol{\theta}) \mu_i L_j \sigma_i \right], \quad (5)$$

where N is the number of \mathcal{GL} \mathcal{DO} bins. The migration matrix A_{ji} represents the number of events expected in \mathcal{RL} bin j for each $H \rightarrow W^+W^-$ signal event found in the \mathcal{GL} bin i . The expected number of events in bin i are expressed as a product of μ_i , the total integrated luminosity L_j (with three possible values corresponding to the three data sets), and the signal cross section σ_i . Note that here σ_i contains both fiducial and nonfiducial components. The total background contribution in bin j is represented by b_j . The factor $\mathcal{N}(\boldsymbol{\theta})$ incorporates a priori constraints on the nuisance parameters, taken as log-normal distributions for most of the individual $\boldsymbol{\theta}$ elements. Finally, the regularization factor $\mathcal{K}(\boldsymbol{\mu})$, present only in the p_T^H measurement, is constructed as

$$\mathcal{K}(\boldsymbol{\mu}) = \prod_{i=2}^{N-1} \exp\left(\frac{-[(\mu_{i+1} - \mu_i) - (\mu_i - \mu_{i-1})]^2}{2\delta^2}\right), \quad (6)$$

with index i running over \mathcal{GL} \mathcal{DO} bins, penalizing thereby large variations among signal strength modifiers of neighboring bins. The parameter δ controls the strength of the regularization, and is optimized by minimizing the mean of the global correlation coefficient [75] in fits to “Asimov” data sets [76]. The optimal value of δ is found to be 2.50. It should be noted that the regularization term acts as a smoothing constraint on the unfolded distribution. Because the distribution of N_{jet} is discrete, regularization was not applied in the N_{jet} fit.

Nonfiducial signal events are scaled together with the fiducial components, with the distinction between fiducial and nonfiducial parts made only when translating the extracted signal strength modifiers into fiducial differential cross sections, achieved by multiplying the fiducial cross section in a given \mathcal{GL} \mathcal{DO} bin i by the corresponding μ_i . This treatment is chosen because the ratio of nonfiducial to fiducial signal yields expected in this analysis averages across \mathcal{DO} bin to ≈ 0.2 . This value is significantly larger than for the diphoton and two Z boson decay channels, rendering the scaling of just the fiducial component unphysical. Nonfiducial signal events appear in the signal region mostly through the discrepancy between \mathcal{GL} and \mathcal{RL} p_T^{miss} affecting m_T^l and m_T^H . In addition, for larger values of N_{jet} , the leading Higgs boson production mode is $t\bar{t}H$, which has more possible $e^\pm \mu^\mp$ final-state configurations where the lepton pair does not arise from $H \rightarrow W^+W^-$ decay. The ratio of nonfiducial over fiducial signal yields is however still affected by the uncertainties on the migration matrix, allowing it to vary postfit with respect to its prefit value.

A RIVET [77] implementation of the STXS scheme [52] is used to compute the \mathcal{GL} p_T^H and N_{jet} observables. For N_{jet} , all final-state particles from the primary interaction, excluding the

Table 2: Binning of the \mathcal{DO} and signal categorizations used in the respective bins.

	p_T^H					
Binning (GeV):	0–20	20–45	45–80	80–120	120–200	>200
Categorization:	4 \mathcal{W}	4 \mathcal{W}	4 \mathcal{W}	3 \mathcal{W}	2 \mathcal{W}	2 \mathcal{W}
	N_{jet}					
Binning:	0	1	2	3	≥ 4	
Categorization:	4 \mathcal{W}	4 \mathcal{W}	2 \mathcal{W}	1 \mathcal{W}	1 \mathcal{W}	

Table 3: Acceptance of each $\mathcal{GL} p_T^H$ bin with its theoretical uncertainty.

p_T^H (GeV)	Acceptance per production mode (%)				
	All SM	ggF	VBF	VH	t \bar{t} H
0–20	6.77 ± 0.36	6.79 ± 0.37	6.57 ± 0.13	4.99 ± 0.12	11.3 ± 1.1
20–45	6.32 ± 0.30	6.33 ± 0.33	6.31 ± 0.09	4.91 ± 0.08	11.1 ± 1.1
45–80	5.94 ± 0.42	5.91 ± 0.53	5.86 ± 0.08	4.81 ± 0.06	10.9 ± 1.0
80–120	6.13 ± 0.47	5.99 ± 0.73	5.77 ± 0.08	5.21 ± 0.07	11.1 ± 1.1
120–200	6.35 ± 0.59	5.84 ± 1.06	5.87 ± 0.09	5.74 ± 0.08	11.4 ± 1.1
>200	6.89 ± 0.73	5.87 ± 1.47	6.22 ± 0.15	6.43 ± 0.17	11.9 ± 1.1

Table 4: Acceptance of each $\mathcal{GL} N_{\text{jet}}$ bin with its theoretical uncertainty.

N_{jet}	Acceptance per production mode (%)				
	All SM	ggF	VBF	VH	t \bar{t} H
0	6.50 ± 0.35	6.58 ± 0.37	6.12 ± 0.11	4.98 ± 0.06	12.5 ± 1.3
1	6.03 ± 0.64	6.04 ± 0.76	5.91 ± 0.08	5.24 ± 0.07	12.5 ± 1.2
2	6.36 ± 0.72	6.08 ± 1.24	5.99 ± 0.08	5.44 ± 0.07	12.5 ± 1.2
3	7.08 ± 0.73	6.26 ± 1.30	6.11 ± 0.11	5.60 ± 0.10	11.5 ± 1.1
≥ 4	7.54 ± 0.66	6.16 ± 1.45	6.03 ± 0.20	5.51 ± 0.15	10.3 ± 1.0

products from Higgs boson decay, are clustered using the anti- k_T algorithm with a distance parameter $R = 0.4$, and jets with $p_T > 30 \text{ GeV}$ are counted regardless of their rapidity.

The binning in both p_T^H and N_{jet} is common for the fiducial space and for the reconstructed events. Bin definitions and categorizations of the reconstructed events within each bin are summarized in Table 2. The bin widths at lower values of p_T^H are dictated by the reconstruction resolution of p_T^{miss} that affects the resolution of p_T^H . At higher values, boundaries are chosen so that the expected uncertainties in μ_i are less than unity. The fraction of events reconstructed in the correct \mathcal{GL} bin ranges from 52 to 73% when spanning from the lowest to the highest p_T^H bin, and the purity of each p_T^H bin, i.e., the fraction of events in \mathcal{RL} bin i that also belong to \mathcal{GL} bin i , ranges from 48 to 80%. Corresponding numbers for the N_{jet} measurement are 80 to 92% and 68 to 95%, respectively, with the highest jet multiplicity bins representing the lowest bound of these intervals.

The values of the signal acceptance per $\mathcal{GL} \mathcal{DO}$ bin are shown in Tables 3 and 4 for p_T^H and N_{jet} respectively.

The two-dimensional histograms of (m^{ll}, m_T^H) in the signal region have different binnings depending on the expected number of events and statistical uncertainties in the templates. The finest binning is 10–25, 25–40, 40–50, 50–70, 70–90, and $>90 \text{ GeV}$ in m^{ll} ; and 60–80, 80–90, 90–110, 110–130, 130–150, and $>150 \text{ GeV}$ in m_T^H . The coarsest binning, used for the highest p_T^H bins,

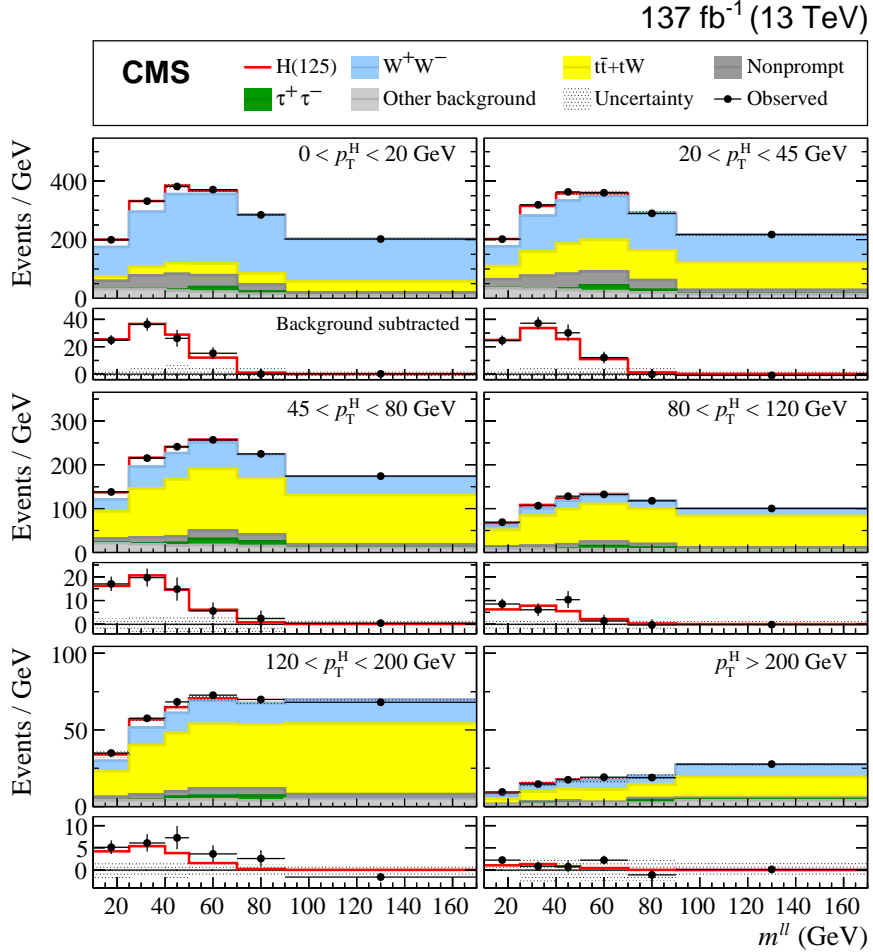


Figure 1: Observed distributions of m^{ll} in data and the expectations from the best fit model with the uncertainties. The distributions in each p_T^H bin are given in separate panels. Within each panel, the lower sub-panel displays background-subtracted observations and expectations.

is 10–50 and >50 GeV in m^{ll} and 60–110 and >110 GeV in m_T^H .

The observed events are shown as a function of m^{ll} in Figs. 1 and 2, along with the predictions from the best fit model and their estimated overall uncertainties. The m^{ll} distributions are formed by integrating the two-dimensional (m^{ll}, m_T^H) distributions and templates over m_T^H and combining all signal regions and all data sets. The yield breakdown in each $\mathcal{RL}\ \mathcal{DO}$ bin is shown in Tables 5 and 6 for the p_T^H and N_{jet} case respectively.

8 Systematic uncertainties

The experimental uncertainties mostly concern the accuracy in modeling the detector response in MC simulation, while the theoretical uncertainties are more specific to individual signal and background processes. Because signal extraction is performed using templates of (m^{ll}, m_T^H) distributions, the relevant effects of the uncertainties are changes in the shapes and normalizations of the templates. In the signal extraction fit, one continuous constrained nuisance parameter

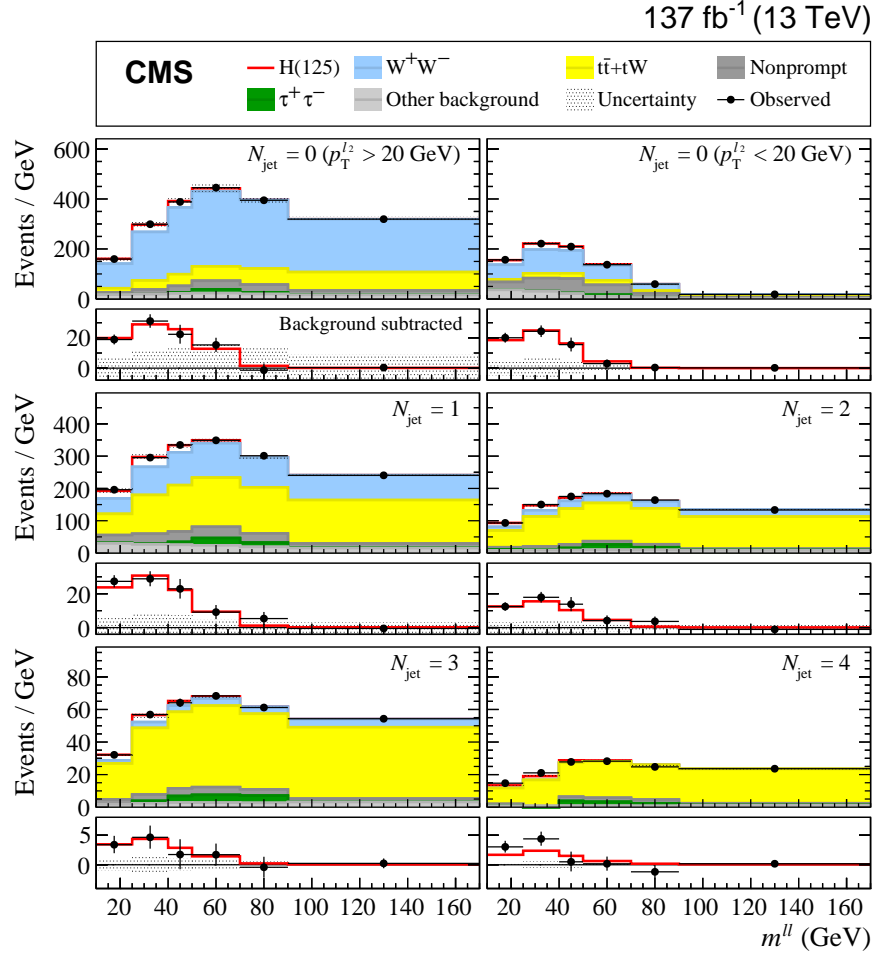


Figure 2: Observed distributions of m^{ll} in data and the expectations from the best fit model with the uncertainties. The distributions in each N_{jet} bin are given in separate panels. Within each panel, the lower sub-panel displays background-subtracted observations and expectations. For $N_{\text{jet}} = 0$, results are split into $p_T^{l_2} > 20 \text{ GeV}$ (left) and $p_T^{l_2} < 20 \text{ GeV}$ (right).

Table 5: Signal and background post-fit (pre-fit) yields in the $\mathcal{RL} p_T^H$ bins.

Process	$\mathcal{RL} p_T^H$ bin						
	[0-20]	[20-45]	[45-80]	[80-120]	[120-200]	> 200	
Data	41032	41799	31273	16942	10366	3514	
H(125)	1485 ± 81 (1356)	1386 ± 80 (1402)	835 ± 52 (792)	320 ± 36 (344)	217 ± 33 (222)	54 ± 17 (75)	
All background	39532 ± 280 (35861)	40414 ± 391 (41978)	30423 ± 393 (32293)	16614 ± 351 (17809)	10154 ± 220 (10790)	3475 ± 107 (4019)	
$\tau^+\tau^-$	537 ± 49 (372)	675 ± 43 (585)	684 ± 61 (482)	316 ± 42 (195)	173 ± 24 (219)	104 ± 58 (83)	
W^+W^-	26945 ± 213 (22840)	17421 ± 290 (18771)	7444 ± 269 (9048)	2759 ± 250 (3972)	2205 ± 155 (2816)	1037 ± 70 (1637)	
$t\bar{t} + tW$	5571 ± 65 (5492)	14700 ± 176 (14528)	18313 ± 239 (18188)	11482 ± 220 (11624)	6481 ± 137 (6488)	1659 ± 40 (1671)	
Nonprompt	3709 ± 127 (5154)	4373 ± 128 (5909)	1822 ± 107 (3143)	1002 ± 80 (1239)	558 ± 52 (749)	197 ± 23 (279)	
Other background	2770 ± 102 (2002)	3245 ± 137 (2186)	2160 ± 100 (1431)	1055 ± 64 (778)	737 ± 49 (519)	478 ± 33 (349)	

Table 6: Signal and background post-fit (pre-fit) yields in the $\mathcal{RL} N_{\text{jet}}$ bins.

Process	$\mathcal{RL} N_{\text{jet}}$ bin				
	0	1	2	3	≥ 4
Data	66263	42959	23027	8912	3765
H(125)	2186 \pm 92 (2447)	1254 \pm 60 (1165)	632 \pm 66 (445)	178 \pm 48 (109)	98 \pm 26 (36)
All background	64085 \pm 463 (63221)	41650 \pm 374 (43994)	22367 \pm 344 (22782)	8735 \pm 182 (8658)	3655 \pm 79 (3822)
$\tau^+ \tau^-$	740 \pm 41 (520)	944 \pm 50 (822)	688 \pm 99 (301)	255 \pm 43 (135)	100 \pm 50 (70)
$W^+ W^-$	41058 \pm 360 (38437)	13190 \pm 252 (15176)	3402 \pm 222 (4266)	698 \pm 125 (966)	0 \pm 0 (240)
$t\bar{t}$ + tW	11125 \pm 144 (11870)	20891 \pm 179 (21198)	15788 \pm 214 (15381)	6853 \pm 110 (6510)	3152 \pm 52 (3031)
Nonprompt	6649 \pm 188 (8999)	3436 \pm 149 (4457)	1066 \pm 77 (1792)	480 \pm 52 (685)	254 \pm 30 (357)
Other background	4513 \pm 165 (3394)	3189 \pm 139 (2342)	1424 \pm 89 (1043)	449 \pm 32 (362)	149 \pm 12 (124)

represents each such change. The constraints are implemented through log-normal probability distribution functions, with the nominal values of the nuisance parameters at zero and the widths given by the estimated sizes of the corresponding uncertainties.

Experimental uncertainties pertaining to all MC simulation samples, both signal and background, are the uncertainties in trigger efficiency, lepton reconstruction and identification efficiencies, lepton momentum scale, jet energy scale, and the uncertainty on p_T^{miss} arising from the momentum scale of low p_T PF candidates not clustered into jets (unclustered energy). Uncertainties in lepton momentum and jet energy scales also affect p_T^{miss} . Each of these uncertainties is represented by one independent nuisance parameter per data set, effectively keeping the template variations for the three data sets in the simultaneous fit uncorrelated. The uncertainty in b tagging efficiency, also included in this class of uncertainties, is represented by seventeen nuisance parameters. Five of these nuisance parameters relate to theoretical predictions of jet flavors involved in the measurement of the efficiency and are thus common among the three data sets. The remaining twelve parameters, four per data set, relate to statistical uncertainties in the samples used to measure the efficiency, and are uncorrelated among the data sets [32].

Uncertainties in the trigger efficiency, and lepton reconstruction and identification efficiencies, evaluated as functions of lepton p_T and η , cause variations in both the shape and the normalization of the templates. The impacts on the template normalizations from the uncertainties in the trigger efficiency are less than 1% overall, while the uncertainties in the reconstruction and identification efficiency cause shape and normalization changes of $\approx 1\%$ for electrons and $\approx 2\%$ for muons. These uncertainties are dominated by the statistical fluctuations of the data set where they are measured, and are thus kept uncorrelated among the data sets.

Changes in the lepton momentum scale, the jet energy scale, and the unclustered energy scale all cause migrations of simulated events between template bins and migration in and out of the acceptance, which in turn cause changes in the shape and normalization of the templates. The impact on the template normalization is $\approx 0.6\text{--}1.0\%$ in the electron momentum scale, 0.2% in the muon momentum scale, and 1–10% in p_T^{miss} . For the changes in the jet energy scale, the impact on the template normalization is ≈ 3 and 10% in the p_T^H and N_{jet} measurements, respectively. The latter has larger uncertainties because the jet energy scale directly affects the number of events falling into different $\mathcal{RL} N_{\text{jet}}$ bins.

There are also experimental uncertainties in the estimation of the nonprompt lepton background. This background is affected by shape uncertainties arising from the dependence of the fake-lepton factors on the flavor composition of the jets misidentified as leptons. These shape uncertainties amount to $\approx 5\text{--}10\%$ (see Ref. [13] for details). Additionally, a 30% normalization uncertainty is assigned to the fit template for the nonprompt lepton background from a closure test performed on simulation. Because these uncertainties depend on lepton reconstruction and identification algorithms, which have differences among the three data sets, they

are represented through independent sets of nuisance parameters. Due to the difference in shape between the nonprompt lepton background and the other backgrounds and the signal, the normalization uncertainty is constrained post-fit to about 50% of its pre-fit value.

The uncertainties in the integrated luminosity are incorporated into the fit as changes in normalization of the templates of the MC simulation samples, excluding the W^+W^- , $t\bar{t} + tW$, and $\tau^+\tau^-$ samples. The total uncertainty in the CMS luminosity is 2.5, 2.3, and 2.5% for the 2016, 2017, and 2018 data sets, respectively [35–37]. These evaluations are partly independent, but also depend on inputs that are common among the three data sets. In total, nine nuisance parameters are introduced to model the correlation in the uncertainties of the integrated luminosity among the data sets.

Several theoretical uncertainties are relevant to all MC simulation samples. Uncertainties in this category arise from the choice of the PDFs, missing higher-order corrections in the perturbative expansion of the simulated cross sections, and modeling of the pileup. Template fluctuations due to these uncertainties are controlled through nuisance parameters common to all three data sets.

Since the changes in the shapes of the templates from the uncertainties in PDFs are found to be small, only the normalization changes, both as cross section changes and acceptance changes, are considered from this source. For the $t\bar{t} + tW$ and $\tau^+\tau^-$ events, while uncertainties in the overall normalizations have no impact in the fit, uncertainties in PDFs give rise to respective 1% and 2% uncertainties in the ratios of the predicted yields in the signal and the control region.

Except for the ggF signal and W^+W^- background processes, the estimated uncertainties from missing higher-order corrections in the perturbative QCD expansion are given by the bin-by-bin difference between the nominal and alternative templates, which are constructed from simulated events, where renormalization and factorization scales are changed up and down by factors of two. Extreme variations where one scale is scaled up and the other is scaled down are excluded. For the ggF signal, the uncertainties are decomposed into several components, such as overall normalization and event migrations between jet multiplicity bins [52]. For the W^+W^- background, the higher-order corrections described in Section 3 are modified by shifting the renormalization and factorization scales and the jet veto threshold, where the latter determines the scale below which QCD gluon radiation is resummed. The entire size of the electroweak corrections to the W^+W^- process is taken as an uncertainty. For the uncertainties in both the PDF and higher-order corrections, processes sharing similar QCD interactions are controlled through a common nuisance parameter.

The uncertainty in the modeling of the pileup is assessed by changing the pp total inelastic cross section of 69.2 mb [78, 79] within a 5% uncertainty, accounting for both the uncertainty in inelastic cross section measurement and the differences in primary vertex reconstruction efficiency between simulation and data.

Theoretical uncertainties in modeling the PS and UE primarily affect the jet multiplicity and are in principle relevant to all MC simulated samples, but in practice have nonnegligible impacts on the fit result only in the ggF and VBF signal samples and the quark-induced W^+W^- background sample. The uncertainty in the PS is evaluated by employing an alternative PS MC generator (HERWIG++ v2.7.1 [80, 81]) for the simulation of the 2016 data set, and by assigning PS variation weights computed in PYTHIA [82] to the simulated events for the simulation of the 2017 and 2018 data sets. The UE uncertainty is evaluated by changing the fit templates using MC simulation samples with UE tunes that are varied from the nominal tunes to cover their uncertainties [42, 43]. For each of the PS and UE uncertainties, changes in the 2017 and 2018

simulations are controlled through one nuisance parameter, but the 2016 simulation uses an independent parameter.

In addition, there are theoretical systematic uncertainties specific to individual background processes. The W^+W^- background events have a 15% uncertainty in the relative fraction of the gluon-induced component [63]. Similarly, the $t\bar{t} + tW$ background events have an uncertainty of 8% in the fraction of the single top quark component. Also the $t\bar{t} + tW$ background sample considers the entire p_T correction weight (as mentioned in Section 3) as the uncertainty in its $t\bar{t}$ component. The $W\gamma^*$ process is assigned a 30% uncertainty arising from the statistical precision of the trilepton control region used to estimate the scale factor assigned to this background process, as described in Section 3.

The theoretical uncertainties reflect those in the cross sections expected for signal processes, as well as their template shapes. Because this analysis is a measurement of fiducial differential cross sections, theoretical uncertainties in the fiducial cross section of each bin of \mathcal{DO} must be excluded from the fits. This is achieved by keeping the normalizations of the signal templates for individual \mathcal{GL} \mathcal{DO} bins constant when changing the values of the nuisance parameters corresponding to theoretical uncertainties.

It should be recognized that the use of regularization in signal extraction can introduce systematic biases in the measured differential cross sections. In particular, by construction, a discrepancy from the expectation in a single \mathcal{DO} bin will be suppressed if the neighboring bins do not exhibit discrepancies in the same direction. The scale of possible regularization bias is measured from the results of the fit as outlined in Ref. [83]. In this method a toy data sample is created with signal yields corresponding to a statistical fluctuation around the best fit model. For each \mathcal{DO} bin the difference in the number of events between the regularized fit result to the toy sample and the toy sample itself is taken as an indication of the scale of bias introduced by regularization. These differences are then translated to estimates of the bias in signal strengths through a multiplication by the rate of change of the extracted signal strength modifiers, estimated by comparing the regularized fit result and the toy data sample. Estimated biases from regularization are separately reported in Section 9 with the measured differential cross sections and other uncertainties. Unfolding bias has also been estimated as the difference between the true and fitted signal strength on an Asimov dataset constructed with either no VBF component or twice the expected VBF component. In this case the bias was smaller than the one estimated with the previously described method.

9 Results

Tables 7 and 8 display the SM cross sections, observed values of μ , the uncertainties separated according to their origin, and the observed cross sections. The contributions to the uncertainties are categorized as: statistical uncertainties in the observed numbers of events; experimental uncertainties excluding those in the integrated luminosity; theoretical uncertainties related only to signal modeling; other theoretical uncertainties; and the uncertainties in the integrated luminosity. Table 7 also shows the estimates of the regularization bias discussed at the end of Section 8.

Correlations among the signal strength modifiers obtained from the fits are shown in Fig. 3. Because the \mathcal{GL} and \mathcal{RL} \mathcal{DO} are not perfectly aligned, the signal template for a \mathcal{GL} bin has nonzero contributions in neighboring \mathcal{RL} bins. This misalignment induces negative correlations between the signal strength modifiers of the nearest-neighbor bins in the fit, which are indeed observed in the correlation matrices. Regularization counters this negative correlation,

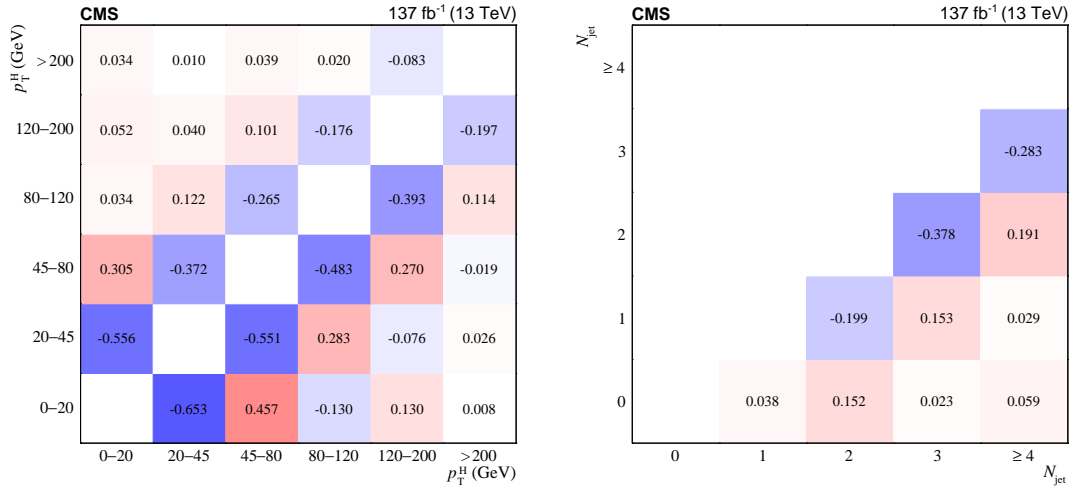


Figure 3: Correlation among the signal strength modifiers in bins of fiducial p_T^H (left) and N_{jet} (right). For the p_T^H matrix, results of the regularized and unregularized fits are given above and below the diagonal.

as evident in the correlation matrix for the p_T^H fit.

The observed cross sections are compared with SM expectations in Fig. 4. As discussed in Section 3, all samples in the nominal signal model are generated using POWHEG, with the ggF component reweighted to match NNLO accuracy. Expectations from an alternative signal model, where the MADGRAPH5_aMC@NLO generator is used for the ggF and VBF components but the VH and $t\bar{t}H$ components are kept identical, are also overlaid in the figure. The largest deviation from the SM prediction is observed in the ≥ 4 jet multiplicity bin and is 1.4 standard deviations.

In addition, the total fiducial cross section is extracted from a fit where the signal in Eq. 5 is reformulated to

$$s'_j(\mu^{\text{fid}}, \rho; \theta) = s_j(\mu^{\text{fid}} \rho; \theta) = \mu^{\text{fid}} \sum_i [A_{ji}(\theta) \rho_i L_j \sigma_i], \quad (7)$$

Table 7: Observed signal strength modifiers and resulting cross sections in fiducial p_T^H bins. The cross section values are the products of σ^{SM} and the regularized μ . The total uncertainty and the contributions by origin are given, where the contributions are statistical (stat), experimental excluding integrated luminosity (exp), theoretical related only to signal modeling (sig), to the background modeling (bkg), and integrated luminosity (lumi). Estimated biases in regularization are separately listed in the second from last column and are not included in the total uncertainty.

p_T^H (GeV)	σ^{SM} (fb)	μ	Value	Regularized μ				Bias	σ^{obs} (fb)
				stat	exp	signal	bkg		
0–20	27.45	1.37 ± 0.30	1.26 ± 0.27	± 0.17	± 0.19	± 0.01	± 0.10	± 0.03	$+0.00$
20–45	24.76	0.52 ± 0.42	0.73 ± 0.36	± 0.24	± 0.25	± 0.01	± 0.10	± 0.03	-0.12
45–80	15.28	1.55 ± 0.41	1.30 ± 0.33	± 0.24	± 0.20	± 0.03	± 0.09	± 0.03	-0.03
80–120	7.72	0.49 ± 0.52	0.79 ± 0.42	± 0.32	± 0.25	± 0.02	± 0.08	± 0.03	-0.16
120–200	5.26	$1.34^{+0.51}_{-0.48}$	1.14 ± 0.41	± 0.29	± 0.27	± 0.04	± 0.08	± 0.03	$+0.11$
>200	2.05	$0.64^{+0.63}_{-0.60}$	$0.73^{+0.61}_{-0.57}$	± 0.38	± 0.42	$^{+0.09}_{-0.03}$	± 0.10	± 0.03	$+0.19$

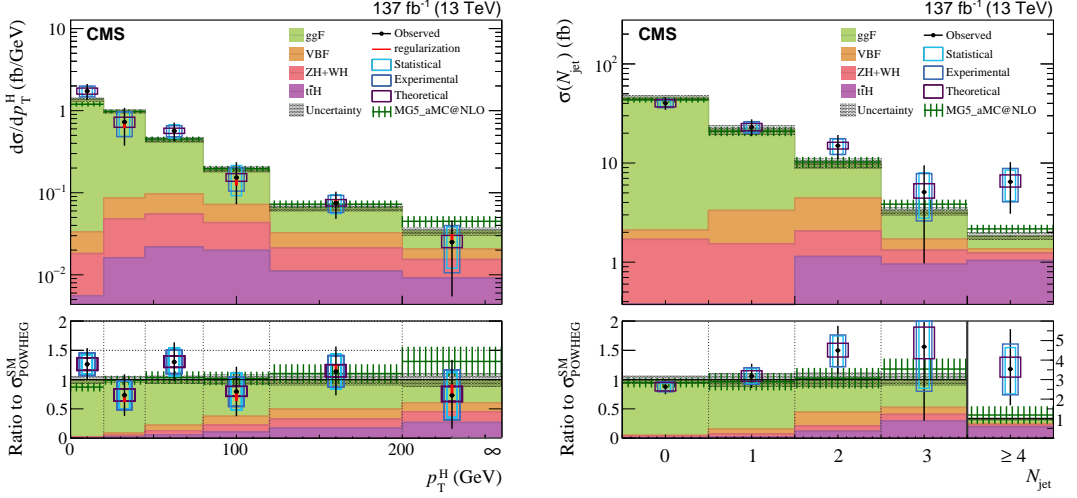


Figure 4: Observed fiducial cross sections in bins of p_T^H (left) and N_{jet} (right), overlaid with predictions from the nominal and alternative models for signal. The ggF and VBF samples are generated using POWHEG in the nominal model and MADGRAPH5_aMC@NLO in the alternative model. The uncertainty bars on the observed cross sections represent the total uncertainty, with the statistical, experimental (including luminosity), and theoretical uncertainties also shown separately. The uncertainty bands on the theoretical predictions correspond to quadratic sums of renormalization- and factorization-scale uncertainties, PDF uncertainties, and statistical uncertainties of the simulation. The filled histograms in the ratio plots show the relative contributions of the Higgs boson production modes in each bin.

in which μ^{fid} and all except one ρ_i are free parameters. A specific ρ_k depends on the other ρ parameters via

$$\rho_k = \frac{\sigma^{\text{SM}} - \sum_{i \neq k} \rho_i \sigma_i^{\text{SM}}}{\sigma_k^{\text{SM}}}, \quad (8)$$

fixing the sum $\sum_i \rho_i \sigma_i^{\text{SM}}$ to the total SM fiducial cross section σ^{SM} , given in Eq. 3. No regularization is applied for this fit. Through this reformulation, anticorrelated components within uncertainties in μ_i are absorbed into the sum $\sum_i A_{ji} \rho_i \sigma_i$, resulting in an uncertainty in μ^{fid} that is smaller than the quadratic sum of uncertainties in individual μ_i that appear in Tables 7 and 8.

The observed signal strength μ^{fid} and cross section $\sigma^{\text{fid}} = \mu^{\text{fid}} \sigma^{\text{SM}}$ from the fit to the p_T^H -binned combined data set, which has a smaller expected uncertainty than the fit to the N_{jet} -binned

Table 8: Observed signal strength modifiers, uncertainties, and resulting cross sections in fiducial N_{jet} bins. The cross section values are the products of σ^{SM} and the unregularized μ . The uncertainties are separated by origin as in Table 7.

N_{jet}	σ^{SM}		μ			σ^{obs}		
	(fb)	Value	stat	exp	signal	bkg	lumi	(fb)
0	45.70	0.88 ± 0.13	± 0.06	± 0.08	± 0.01	± 0.07	± 0.03	40.1 ± 6.0
1	21.74	1.06 ± 0.20	± 0.12	± 0.14	± 0.01	± 0.08	± 0.03	23.0 ± 4.6
2	9.99	1.50 ± 0.40	± 0.25 ± 0.28	± 0.28	± 0.04	± 0.11	± 0.03	15.0 ± 4.2
3	3.26	$1.56^{+1.35}_{-1.26}$	± 0.89 ± 0.71	± 0.84 ± 0.76	± 0.17 ± 0.07	± 0.29 ± 0.19	± 0.07 ± 0.04	$5.1^{+4.4}_{-4.1}$
≥ 4	1.83	$3.54^{+2.05}_{-1.86}$	± 1.10 ± 1.28	± 1.28 ± 1.32	± 0.40 ± 0.20	± 0.38 ± 0.34	± 0.10 ± 0.07	$6.5^{+3.8}_{-3.4}$

combined data set, are

$$\mu^{\text{fid}} = 1.05 \pm 0.12 \left(\pm 0.05 \text{ (stat)} \pm 0.07 \text{ (exp)} \pm 0.01 \text{ (signal)} \pm 0.07 \text{ (bkg)} \pm 0.03 \text{ (lumi)} \right), \quad (9)$$

$$\sigma^{\text{fid}} = 86.5 \pm 9.5 \text{ fb}. \quad (10)$$

where (stat) refers to the statistical uncertainties (including the background normalizations extracted from control regions), (exp) to the experimental uncertainties excluding those in the integrated luminosity, (signal) to the theoretical uncertainties in modeling the signal, (bkg) to the remaining theoretical uncertainties, and (lumi) to the luminosity uncertainty. Tabulated results are available in the HepData database [84].

10 Summary

Inclusive and differential fiducial cross sections for Higgs boson production have been measured using $H \rightarrow W^+W^- \rightarrow e^\pm\mu^\mp\nu\bar{\nu}$ decays. The measurements were performed using pp collisions recorded by the CMS detector at a center-of-mass energy of 13 TeV, corresponding to a total integrated luminosity of 137 fb^{-1} . Differential cross sections as a function of the transverse momentum of the Higgs boson and the number of associated jets produced are determined in a fiducial phase space that is matched to the experimental kinematic acceptance. The cross sections are extracted through a simultaneous fit to kinematic distributions of the signal candidate events categorized to maximize sensitivity to Higgs boson production. The measurements are compared to standard model theoretical calculations using the POWHEG and MADGRAPH5_aMC@NLO generators. No significant deviation from the standard model expectations is observed. The integrated fiducial cross section is measured to be $86.5 \pm 9.5 \text{ fb}$, consistent with the SM expectation of $82.5 \pm 4.2 \text{ fb}$. These measurements were performed for the first time in the $H \rightarrow W^+W^-$ decay channel at $\sqrt{s} = 13 \text{ TeV}$ exploiting the full data sample available. The methods for the determination of the differential cross section have been updated significantly compared to the last report in the same channel at $\sqrt{s} = 8 \text{ TeV}$, combining the signal extraction, unfolding, and regularization into a single simultaneous fit.

Acknowledgments

We congratulate our colleagues in the CERN accelerator departments for the excellent performance of the LHC and thank the technical and administrative staffs at CERN and at other CMS institutes for their contributions to the success of the CMS effort. In addition, we gratefully acknowledge the computing centers and personnel of the Worldwide LHC Computing Grid for delivering so effectively the computing infrastructure essential to our analyses. Finally, we acknowledge the enduring support for the construction and operation of the LHC and the CMS detector provided by the following funding agencies: BMBWF and FWF (Austria); FNRS and FWO (Belgium); CNPq, CAPES, FAPERJ, FAPERGS, and FAPESP (Brazil); MES (Bulgaria); CERN; CAS, MoST, and NSFC (China); COLCIENCIAS (Colombia); MSES and CSF (Croatia); RIF (Cyprus); SENESCYT (Ecuador); MoER, ERC IUT, PUT and ERDF (Estonia); Academy of Finland, MEC, and HIP (Finland); CEA and CNRS/IN2P3 (France); BMBF, DFG, and HGF (Germany); GSRT (Greece); NKFIA (Hungary); DAE and DST (India); IPM (Iran); SFI (Ireland); INFN (Italy); MSIP and NRF (Republic of Korea); MES (Latvia); LAS (Lithuania); MOE and UM (Malaysia); BUAP, CINVESTAV, CONACYT, LNS, SEP, and UASLP-FAI (Mexico); MOS (Montenegro); MBIE (New Zealand); PAEC (Pakistan); MSHE and NSC (Poland); FCT (Portugal);

JINR (Dubna); MON, RosAtom, RAS, RFBR, and NRC KI (Russia); MESTD (Serbia); SEIDI, CPAN, PCTI, and FEDER (Spain); MOSTR (Sri Lanka); Swiss Funding Agencies (Switzerland); MST (Taipei); ThEPCenter, IPST, STAR, and NSTDA (Thailand); TUBITAK and TAEK (Turkey); NASU (Ukraine); STFC (United Kingdom); DOE and NSF (USA).

Individuals have received support from the Marie-Curie program and the European Research Council and Horizon 2020 Grant, contract Nos. 675440, 752730, and 765710 (European Union); the Leventis Foundation; the A.P. Sloan Foundation; the Alexander von Humboldt Foundation; the Belgian Federal Science Policy Office; the Fonds pour la Formation à la Recherche dans l'Industrie et dans l'Agriculture (FRIA-Belgium); the Agentschap voor Innovatie door Wetenschap en Technologie (IWT-Belgium); the F.R.S.-FNRS and FWO (Belgium) under the "Excellence of Science – EOS" – be.h project n. 30820817; the Beijing Municipal Science & Technology Commission, No. Z191100007219010; the Ministry of Education, Youth and Sports (MEYS) of the Czech Republic; the Deutsche Forschungsgemeinschaft (DFG) under Germany's Excellence Strategy – EXC 2121 "Quantum Universe" – 390833306; the Lendület ("Momentum") Program and the János Bolyai Research Scholarship of the Hungarian Academy of Sciences, the New National Excellence Program ÚNKP, the NKFIA research grants 123842, 123959, 124845, 124850, 125105, 128713, 128786, and 129058 (Hungary); the Council of Science and Industrial Research, India; the HOMING PLUS program of the Foundation for Polish Science, cofinanced from European Union, Regional Development Fund, the Mobility Plus program of the Ministry of Science and Higher Education, the National Science Center (Poland), contracts Harmonia 2014/14/M/ST2/00428, Opus 2014/13/B/ST2/02543, 2014/15/B/ST2/03998, and 2015/19/B/ST2/02861, Sonata-bis 2012/07/E/ST2/01406; the National Priorities Research Program by Qatar National Research Fund; the Ministry of Science and Higher Education, project no. 02.a03.21.0005 (Russia); the Programa Estatal de Fomento de la Investigación Científica y Técnica de Excelencia María de Maeztu, grant MDM-2015-0509 and the Programa Severo Ochoa del Principado de Asturias; the Thalis and Aristeia programs cofinanced by EU-ESF and the Greek NSRF; the Rachadapisek Sompot Fund for Postdoctoral Fellowship, Chulalongkorn University and the Chulalongkorn Academic into Its 2nd Century Project Advancement Project (Thailand); the Kavli Foundation; the Nvidia Corporation; the SuperMicro Corporation; the Welch Foundation, contract C-1845; and the Weston Havens Foundation (USA).

References

- [1] ATLAS Collaboration, "Observation of a new particle in the search for the standard model Higgs boson with the ATLAS detector at the LHC", *Phys. Lett. B* **716** (2012) 1, doi:10.1016/j.physletb.2012.08.020, arXiv:1207.7214.
- [2] CMS Collaboration, "Observation of a new boson at a mass of 125 GeV with the CMS experiment at the LHC", *Phys. Lett. B* **716** (2012) 30, doi:10.1016/j.physletb.2012.08.021, arXiv:1207.7235.
- [3] CMS Collaboration, "Observation of a new boson with mass near 125 GeV in pp collisions at $\sqrt{s} = 7$ and 8 TeV", *JHEP* **06** (2013) 081, doi:10.1007/JHEP06(2013)081, arXiv:1303.4571.
- [4] P. F. Monni et al., "MiNNLO_{PS}: a new method to match NNLO QCD to parton showers", *JHEP* **05** (2020) 143, doi:10.1007/JHEP05(2020)143, arXiv:1908.06987.
- [5] S. P. Jones, M. Kerner, and G. Luisoni, "Next-to-leading-order QCD corrections to Higgs boson plus jet production with full top-quark mass dependence", *Phys. Rev. Lett.* **120**

- (2018), no. 16, 162001, doi:10.1103/PhysRevLett.120.162001, arXiv:1802.00349.
- [6] K. Hamilton, P. Nason, and G. Zanderighi, “Finite quark-mass effects in the NNLOPS POWHEG+MiNLO Higgs generator”, *JHEP* **05** (2015) 140, doi:10.1007/JHEP05(2015)140, arXiv:1501.04637.
- [7] K. Hamilton, P. Nason, E. Re, and G. Zanderighi, “NNLOPS simulation of Higgs boson production”, *JHEP* **10** (2013) 222, doi:10.1007/JHEP10(2013)222, arXiv:1309.0017.
- [8] M. Cacciari et al., “Fully Differential Vector-Boson-Fusion Higgs Production at Next-to-Next-to-Leading Order”, *Phys. Rev. Lett.* **115** (2015), no. 8, 082002, doi:10.1103/PhysRevLett.115.082002, arXiv:1506.02660. [Erratum: *Phys.Rev.Lett.* **120**, 139901 (2018)].
- [9] S. Alioli et al., “Higgsstrahlung at NNLL' + NNLO matched to parton showers in GENEVA”, *Phys. Rev. D* **100** (2019) 096016, doi:10.1103/PhysRevD.100.096016, arXiv:1909.02026.
- [10] F. Bishara, U. Haisch, P. F. Monni, and E. Re, “Constraining light-quark Yukawa couplings from Higgs distributions”, *Phys. Rev. Lett.* **118** (2017) 121801, doi:10.1103/PhysRevLett.118.121801, arXiv:1606.09253.
- [11] M. Grazzini, A. Ilnicka, M. Spira, and M. Wiesemann, “Modeling BSM effects on the Higgs transverse-momentum spectrum in an EFT approach”, *JHEP* **03** (2017) 115, doi:10.1007/JHEP03(2017)115, arXiv:1612.00283.
- [12] ATLAS Collaboration, “Measurements of gluon-gluon fusion and vector-boson fusion Higgs boson production cross-sections in the $H \rightarrow WW^* \rightarrow e\nu\mu\nu$ decay channel in pp collisions at $\sqrt{s} = 13$ TeV with the ATLAS detector”, *Phys. Lett. B* **789** (2019) 508, doi:10.1016/j.physletb.2018.11.064, arXiv:1808.09054.
- [13] CMS Collaboration, “Measurements of properties of the Higgs boson decaying to a W boson pair in pp collisions at $\sqrt{s} = 13$ TeV”, *Phys. Lett. B* **791** (2019) 96, doi:10.1016/j.physletb.2018.12.073, arXiv:1806.05246.
- [14] ATLAS Collaboration, “Combined measurement of differential and total cross sections in the $H \rightarrow \gamma\gamma$ and the $H \rightarrow ZZ^* \rightarrow 4\ell$ decay channels at $\sqrt{s} = 13$ TeV with the ATLAS detector”, *Phys. Lett. B* **786** (2018) 114, doi:10.1016/j.physletb.2018.09.019, arXiv:1805.10197.
- [15] CMS Collaboration, “Measurement and interpretation of differential cross sections for Higgs boson production at $\sqrt{s} = 13$ TeV”, *Phys. Lett. B* **792** (2019) 369, doi:10.1016/j.physletb.2019.03.059, arXiv:1812.06504.
- [16] CMS Collaboration, “Measurement of inclusive and differential Higgs boson production cross sections in the diphoton decay channel in proton-proton collisions at $\sqrt{s} = 13$ TeV”, *JHEP* **01** (2019) 183, doi:10.1007/JHEP01(2019)183, arXiv:1807.03825.
- [17] CMS Collaboration, “Measurements of properties of the Higgs boson decaying into the four-lepton final state in pp collisions at $\sqrt{s} = 13$ TeV”, *JHEP* **11** (2017) 047, doi:10.1007/JHEP11(2017)047, arXiv:1706.09936.

- [18] CMS Collaboration, “Inclusive search for a highly boosted Higgs boson decaying to a bottom quark-antiquark pair”, *Phys. Rev. Lett.* **120** (2018), no. 7, 071802, doi:10.1103/PhysRevLett.120.071802, arXiv:1709.05543.
- [19] ATLAS Collaboration, “Measurement of fiducial differential cross sections of gluon-fusion production of Higgs bosons decaying to $WW^* \rightarrow e\nu\mu\nu$ with the ATLAS detector at $\sqrt{s} = 8$ TeV”, *JHEP* **08** (2016) 104, doi:10.1007/JHEP08(2016)104, arXiv:1604.02997.
- [20] CMS Collaboration, “Measurement of the transverse momentum spectrum of the Higgs boson produced in pp collisions at $\sqrt{s} = 8$ TeV using $H \rightarrow WW$ decays”, *JHEP* **03** (2017) 032, doi:10.1007/JHEP03(2017)032, arXiv:1606.01522.
- [21] CMS Collaboration, “The CMS trigger system”, *JINST* **12** (2017) P01020, doi:10.1088/1748-0221/12/01/P01020, arXiv:1609.02366.
- [22] CMS Collaboration, “The CMS experiment at the CERN LHC”, *JINST* **3** (2008) S08004, doi:10.1088/1748-0221/3/08/S08004.
- [23] CMS Collaboration, “Performance of electron reconstruction and selection with the CMS detector in proton-proton collisions at $\sqrt{s} = 8$ TeV”, *JINST* **10** (2015) P06005, doi:10.1088/1748-0221/10/06/P06005, arXiv:1502.02701.
- [24] CMS Collaboration, “Performance of the CMS muon detector and muon reconstruction with proton-proton collisions at $\sqrt{s} = 13$ TeV”, *JINST* **13** (2018) P06015, doi:10.1088/1748-0221/13/06/P06015, arXiv:1804.04528.
- [25] CMS Collaboration, “Performance of the reconstruction and identification of high-momentum muons in proton-proton collisions at $\sqrt{s} = 13$ TeV”, *JINST* **15** (2020) P02027, doi:10.1088/1748-0221/15/02/P02027, arXiv:1912.03516.
- [26] W. Waltenberger, R. Fröhwirth, and P. Vanlaer, “Adaptive vertex fitting”, *J. Phys. G* **34** (2007) N343, doi:10.1088/0954-3899/34/12/N01.
- [27] M. Cacciari, G. P. Salam, and G. Soyez, “The anti- k_T jet clustering algorithm”, *JHEP* **04** (2008) 063, doi:10.1088/1126-6708/2008/04/063, arXiv:0802.1189.
- [28] M. Cacciari, G. P. Salam, and G. Soyez, “FastJet user manual”, *Eur. Phys. J. C* **72** (2012) 1896, doi:10.1140/epjc/s10052-012-1896-2, arXiv:1111.6097.
- [29] CMS Collaboration, “Particle-flow reconstruction and global event description with the CMS detector”, *JINST* **12** (2017) P10003, doi:10.1088/1748-0221/12/10/P10003, arXiv:1706.04965.
- [30] CMS Collaboration, “Jet energy scale and resolution in the CMS experiment in pp collisions at 8 TeV”, *JINST* **12** (2017) P02014, doi:10.1088/1748-0221/12/02/P02014, arXiv:1607.03663.
- [31] CMS Collaboration, “Jet energy scale and resolution performance with 13 TeV data collected by CMS in 2016-2018”, CMS Detector Performance Summary CMS-DP-2020-019, 2020.
- [32] CMS Collaboration, “Identification of heavy-flavour jets with the CMS detector in pp collisions at 13 TeV”, *JINST* **13** (2018) P05011, doi:10.1088/1748-0221/13/05/P05011, arXiv:1712.07158.

- [33] CMS Collaboration, “Performance of missing transverse momentum reconstruction in proton-proton collisions at $\sqrt{s} = 13$ TeV using the CMS detector”, *JINST* **14** (2019) P07004, doi:10.1088/1748-0221/14/07/P07004, arXiv:1903.06078.
- [34] D. Bertolini, P. Harris, M. Low, and N. Tran, “Pileup per particle identification”, *JHEP* **10** (2014) 059, doi:10.1007/JHEP10(2014)059, arXiv:1407.6013.
- [35] CMS Collaboration, “CMS luminosity measurements for the 2016 data-taking period”, CMS Physics Analysis Summary CMS-PAS-LUM-17-001, 2017.
- [36] CMS Collaboration, “CMS luminosity measurement for the 2017 data-taking period at $\sqrt{s} = 13$ TeV”, CMS Physics Analysis Summary CMS-PAS-LUM-17-004, 2017.
- [37] CMS Collaboration, “CMS luminosity measurement for the 2018 data-taking period at $\sqrt{s} = 13$ TeV”, CMS Physics Analysis Summary CMS-PAS-LUM-18-002, 2019.
- [38] T. Sjöstrand et al., “An introduction to PYTHIA 8.2”, *Comput. Phys. Commun.* **191** (2015) 159, doi:10.1016/j.cpc.2015.01.024, arXiv:1410.3012.
- [39] NNPDF Collaboration, “Parton distributions with QED corrections”, *Nucl. Phys. B* **877** (2013) 290, doi:10.1016/j.nuclphysb.2013.10.010, arXiv:1308.0598.
- [40] NNPDF Collaboration, “Unbiased global determination of parton distributions and their uncertainties at NNLO and at LO”, *Nucl. Phys. B* **855** (2012) 153, doi:10.1016/j.nuclphysb.2011.09.024, arXiv:1107.2652.
- [41] NNPDF Collaboration, “Parton distributions from high-precision collider data”, *Eur. Phys. J. C* **77** (2017) 663, doi:10.1140/epjc/s10052-017-5199-5, arXiv:1706.00428.
- [42] CMS Collaboration, “Event generator tunes obtained from underlying event and multiparton scattering measurements”, *Eur. Phys. J. C* **76** (2016) 155, doi:10.1140/epjc/s10052-016-3988-x, arXiv:1512.00815.
- [43] CMS Collaboration, “Extraction and validation of a new set of CMS PYTHIA8 tunes from underlying-event measurements”, *Eur. Phys. J. C* **80** (2020) 4, doi:10.1140/epjc/s10052-019-7499-4, arXiv:1903.12179.
- [44] P. Nason, “A new method for combining NLO QCD with shower Monte Carlo algorithms”, *JHEP* **11** (2004) 040, doi:10.1088/1126-6708/2004/11/040, arXiv:hep-ph/0409146.
- [45] S. Frixione, P. Nason, and C. Oleari, “Matching NLO QCD computations with parton shower simulations: the POWHEG method”, *JHEP* **11** (2007) 070, doi:10.1088/1126-6708/2007/11/070, arXiv:0709.2092.
- [46] S. Alioli, P. Nason, C. Oleari, and E. Re, “A general framework for implementing NLO calculations in shower Monte Carlo programs: the POWHEG BOX”, *JHEP* **06** (2010) 043, doi:10.1007/JHEP06(2010)043, arXiv:1002.2581.
- [47] E. Bagnaschi, G. Degrassi, P. Slavich, and A. Vicini, “Higgs production via gluon fusion in the POWHEG approach in the SM and in the MSSM”, *JHEP* **02** (2012) 088, doi:10.1007/JHEP02(2012)088, arXiv:1111.2854.

- [48] P. Nason and C. Oleari, “NLO Higgs boson production via vector-boson fusion matched with shower in POWHEG”, *JHEP* **02** (2010) 037, doi:10.1007/JHEP02(2010)037, arXiv:0911.5299.
- [49] G. Luisoni, P. Nason, C. Oleari, and F. Tramontano, “ $\text{HW}^\pm/\text{HZ} + 0$ and 1 jet at NLO with the POWHEG BOX interfaced to GoSam and their merging within MiNLO”, *JHEP* **10** (2013) 083, doi:10.1007/JHEP10(2013)083, arXiv:1306.2542.
- [50] H. B. Hartanto, B. Jager, L. Reina, and D. Wackerlo, “Higgs boson production in association with top quarks in the POWHEG BOX”, *Phys. Rev. D* **91** (2015) 094003, doi:10.1103/PhysRevD.91.094003, arXiv:1501.04498.
- [51] N. Berger et al., “Simplified template cross sections – stage 1.1”, (2019). arXiv:1906.02754.
- [52] LHC Higgs Cross Section Working Group Collaboration, “Handbook of LHC Higgs cross sections: 4. deciphering the nature of the Higgs sector”, (2016). arXiv:1610.07922.
- [53] C. Anastasiou et al., “Higgs boson gluon fusion production beyond threshold in $N^3\text{LO}$ QCD”, *JHEP* **03** (2015) 091, doi:10.1007/JHEP03(2015)091, arXiv:1411.3584.
- [54] C. Anastasiou et al., “Soft expansion of double-real-virtual corrections to Higgs production at $N^3\text{LO}$ ”, *JHEP* **08** (2015) 051, doi:10.1007/JHEP08(2015)051, arXiv:1505.04110.
- [55] C. Anastasiou et al., “High precision determination of the gluon fusion Higgs boson cross-section at the LHC”, *JHEP* **05** (2016) 058, doi:10.1007/JHEP05(2016)058, arXiv:1602.00695.
- [56] J. Alwall et al., “The automated computation of tree-level and next-to-leading order differential cross sections, and their matching to parton shower simulations”, *JHEP* **07** (2014) 079, doi:10.1007/JHEP07(2014)079, arXiv:1405.0301.
- [57] R. Frederix and S. Frixione, “Merging meets matching in MC@NLO”, *JHEP* **12** (2012) 061, doi:10.1007/JHEP12(2012)061, arXiv:1209.6215.
- [58] S. Bolognesi et al., “On the spin and parity of a single-produced resonance at the LHC”, *Phys. Rev. D* **86** (2012) 095031, doi:10.1103/PhysRevD.86.095031, arXiv:1208.4018.
- [59] P. Nason and G. Zanderighi, “ W^+W^- , WZ and ZZ production in the POWHEG-BOX-V2”, *Eur. Phys. J. C* **74** (2014), no. 1, 2702, doi:10.1140/epjc/s10052-013-2702-5, arXiv:1311.1365.
- [60] J. M. Campbell and R. K. Ellis, “An update on vector boson pair production at hadron colliders”, *Phys. Rev. D* **60** (1999) 113006, doi:10.1103/PhysRevD.60.113006, arXiv:hep-ph/9905386.
- [61] J. M. Campbell, R. K. Ellis, and C. Williams, “Vector boson pair production at the LHC”, *JHEP* **07** (2011) 018, doi:10.1007/JHEP07(2011)018, arXiv:1105.0020.
- [62] J. M. Campbell, R. K. Ellis, and W. T. Giele, “A multi-threaded version of MCFM”, *Eur. Phys. J. C* **75** (2015) 246, doi:10.1140/epjc/s10052-015-3461-2, arXiv:1503.06182.

- [63] F. Caola et al., “QCD corrections to vector boson pair production in gluon fusion including interference effects with off-shell Higgs at the LHC”, *JHEP* **07** (2016) 087, doi:[10.1007/JHEP07\(2016\)087](https://doi.org/10.1007/JHEP07(2016)087), arXiv:[1605.04610](https://arxiv.org/abs/1605.04610).
- [64] S. Frixione, P. Nason, and G. Ridolfi, “A Positive-weight next-to-leading-order Monte Carlo for heavy flavour hadroproduction”, *JHEP* **09** (2007) 126, doi:[10.1088/1126-6708/2007/09/126](https://doi.org/10.1088/1126-6708/2007/09/126), arXiv:[0707.3088](https://arxiv.org/abs/0707.3088).
- [65] S. Alioli, P. Nason, C. Oleari, and E. Re, “NLO single-top production matched with shower in POWHEG: s - and t -channel contributions”, *JHEP* **09** (2009) 111, doi:[10.1088/1126-6708/2009/09/111](https://doi.org/10.1088/1126-6708/2009/09/111), arXiv:[0907.4076](https://arxiv.org/abs/0907.4076). [Erratum: doi:[10.1007/JHEP02\(2010\)011](https://doi.org/10.1007/JHEP02(2010)011)].
- [66] E. Re, “Single-top Wt -channel production matched with parton showers using the POWHEG method”, *Eur. Phys. J. C* **71** (2011) 1547, doi:[10.1140/epjc/s10052-011-1547-z](https://doi.org/10.1140/epjc/s10052-011-1547-z), arXiv:[1009.2450](https://arxiv.org/abs/1009.2450).
- [67] P. Meade, H. Ramani, and M. Zeng, “Transverse momentum resummation effects in W^+W^- measurements”, *Phys. Rev. D* **90** (2014) 114006, doi:[10.1103/PhysRevD.90.114006](https://doi.org/10.1103/PhysRevD.90.114006), arXiv:[1407.4481](https://arxiv.org/abs/1407.4481).
- [68] P. Jaiswal and T. Okui, “Explanation of the WW excess at the LHC by jet-veto resummation”, *Phys. Rev. D* **90** (2014) 073009, doi:[10.1103/PhysRevD.90.073009](https://doi.org/10.1103/PhysRevD.90.073009), arXiv:[1407.4537](https://arxiv.org/abs/1407.4537).
- [69] S. Gieseke, T. Kasprzik, and J. H. Kühn, “Vector-boson pair production and electroweak corrections in HERWIG++”, *Eur. Phys. J. C* **74** (2014) 2988, doi:[10.1140/epjc/s10052-014-2988-y](https://doi.org/10.1140/epjc/s10052-014-2988-y), arXiv:[1401.3964](https://arxiv.org/abs/1401.3964).
- [70] CMS Collaboration, “Measurement of differential cross sections for top quark pair production using the lepton+jets final state in proton-proton collisions at 13 TeV”, *Phys. Rev. D* **95** (2017) 092001, doi:[10.1103/PhysRevD.95.092001](https://doi.org/10.1103/PhysRevD.95.092001), arXiv:[1610.04191](https://arxiv.org/abs/1610.04191).
- [71] CMS Collaboration, “Measurements of differential Z boson production cross sections in proton-proton collisions at $\sqrt{s} = 13$ TeV”, *JHEP* **12** (2019) 061, doi:[10.1007/JHEP12\(2019\)061](https://doi.org/10.1007/JHEP12(2019)061), arXiv:[1909.04133](https://arxiv.org/abs/1909.04133).
- [72] GEANT4 Collaboration, “GEANT4—a simulation toolkit”, *Nucl. Instrum. Meth. A* **506** (2003) 250, doi:[10.1016/S0168-9002\(03\)01368-8](https://doi.org/10.1016/S0168-9002(03)01368-8).
- [73] CMS Collaboration, “Measurement of Higgs boson production and properties in the WW decay channel with leptonic final states”, *JHEP* **01** (2014) 096, doi:[10.1007/JHEP01\(2014\)096](https://doi.org/10.1007/JHEP01(2014)096), arXiv:[1312.1129](https://arxiv.org/abs/1312.1129).
- [74] M. Cacciari and G. P. Salam, “Pileup subtraction using jet areas”, *Phys. Lett. B* **659** (2008) 119, doi:[10.1016/j.physletb.2007.09.077](https://doi.org/10.1016/j.physletb.2007.09.077), arXiv:[0707.1378](https://arxiv.org/abs/0707.1378).
- [75] S. Schmitt, “TUnfold: an algorithm for correcting migration effects in high energy physics”, *JINST* **7** (2012) T10003, doi:[10.1088/1748-0221/7/10/T10003](https://doi.org/10.1088/1748-0221/7/10/T10003), arXiv:[1205.6201](https://arxiv.org/abs/1205.6201).
- [76] G. Cowan, K. Cranmer, E. Gross, and O. Vitells, “Asymptotic formulae for likelihood-based tests of new physics”, *Eur. Phys. J. C* **71** (2011) 1554, doi:[10.1140/epjc/s10052-011-1554-0](https://doi.org/10.1140/epjc/s10052-011-1554-0), arXiv:[1007.1727](https://arxiv.org/abs/1007.1727). [Erratum: doi:[10.1140/epjc/s10052-013-2501-z](https://doi.org/10.1140/epjc/s10052-013-2501-z)].

- [77] C. Bierlich et al., “Robust independent validation of experiment and theory: Rivet version 3”, *SciPost Phys.* **8** (2020) 026, doi:10.21468/SciPostPhys.8.2.026, arXiv:1912.05451.
- [78] ATLAS Collaboration, “Measurement of the inelastic proton-proton cross section at $\sqrt{s} = 13 \text{ TeV}$ with the ATLAS detector at the LHC”, *Phys. Rev. Lett.* **117** (2016) 182002, doi:10.1103/PhysRevLett.117.182002, arXiv:1606.02625.
- [79] CMS Collaboration, “Measurement of the inelastic proton-proton cross section at $\sqrt{s} = 13 \text{ TeV}$ ”, *JHEP* **07** (2018) 161, doi:10.1007/JHEP07(2018)161, arXiv:1802.02613.
- [80] M. Bahr et al., “Herwig++ physics and manual”, *Eur. Phys. J. C* **58** (2008) 639, doi:10.1140/epjc/s10052-008-0798-9, arXiv:0803.0883.
- [81] J. Bellm et al., “Herwig 7.0/Herwig++ 3.0 release note”, *Eur. Phys. J. C* **76** (2016) 196, doi:10.1140/epjc/s10052-016-4018-8, arXiv:1512.01178.
- [82] S. Mrenna and P. Skands, “Automated parton-shower variations in PYTHIA 8”, *Phys. Rev. D* **94** (2016) 074005, doi:10.1103/PhysRevD.94.074005, arXiv:1605.08352.
- [83] G. Cowan, “Statistical data analysis”, ch. 11, p. 173. Oxford University Press, 1998.
- [84] “HEPData record for this analysis”. doi:10.17182/hepdata.100162.

A The CMS Collaboration

Yerevan Physics Institute, Yerevan, Armenia

A.M. Sirunyan[†], A. Tumasyan

Institut für Hochenergiephysik, Wien, Austria

W. Adam, F. Ambrogi, T. Bergauer, M. Dragicevic, J. Erö, A. Escalante Del Valle, M. Flechl, R. Frühwirth¹, M. Jeitler¹, N. Krammer, I. Krätschmer, D. Liko, T. Madlener, I. Mikulec, N. Rad, J. Schieck¹, R. Schöfbeck, M. Spanring, W. Waltenberger, C.-E. Wulz¹, M. Zarucki

Institute for Nuclear Problems, Minsk, Belarus

V. Drugakov, V. Mossolov, J. Suarez Gonzalez

Universiteit Antwerpen, Antwerpen, Belgium

M.R. Darwish, E.A. De Wolf, D. Di Croce, X. Janssen, T. Kello², A. Lelek, M. Pieters, H. Rejeb Sfar, H. Van Haevermaet, P. Van Mechelen, S. Van Putte, N. Van Remortel

Vrije Universiteit Brussel, Brussel, Belgium

F. Blekman, E.S. Bols, S.S. Chhibra, J. D'Hondt, J. De Clercq, D. Lontkovskyi, S. Lowette, I. Marchesini, S. Moortgat, Q. Python, S. Tavernier, W. Van Doninck, P. Van Mulders

Université Libre de Bruxelles, Bruxelles, Belgium

D. Beghin, B. Bilin, B. Clerbaux, G. De Lentdecker, H. Delannoy, B. Dorney, L. Favart, A.K. Kalsi, L. Moureaux, A. Popov, N. Postiau, E. Starling, L. Thomas, C. Vander Velde, P. Vanlaer, D. Vannerom

Ghent University, Ghent, Belgium

T. Cornelis, D. Dobur, I. Khvastunov³, M. Niedziela, C. Roskas, K. Skovpen, M. Tytgat, W. Verbeke, B. Vermassen, M. Vit

Université Catholique de Louvain, Louvain-la-Neuve, Belgium

G. Bruno, C. Caputo, P. David, C. Delaere, M. Delcourt, A. Giammacco, V. Lemaitre, J. Prisciandaro, A. Saggio, P. Vischia, J. Zobec

Centro Brasileiro de Pesquisas Fisicas, Rio de Janeiro, Brazil

G.A. Alves, G. Correia Silva, C. Hensel, A. Moraes

Universidade do Estado do Rio de Janeiro, Rio de Janeiro, Brazil

E. Belchior Batista Das Chagas, W. Carvalho, J. Chinellato⁴, E. Coelho, E.M. Da Costa, G.G. Da Silveira⁵, D. De Jesus Damiao, C. De Oliveira Martins, S. Fonseca De Souza, H. Malbouisson, J. Martins⁶, D. Matos Figueiredo, M. Medina Jaime⁷, M. Melo De Almeida, C. Mora Herrera, L. Mundim, H. Nogima, W.L. Prado Da Silva, P. Rebello Teles, L.J. Sanchez Rosas, A. Santoro, A. Sznajder, M. Thiel, E.J. Tonelli Manganote⁴, F. Torres Da Silva De Araujo, A. Vilela Pereira

Universidade Estadual Paulista ^a, Universidade Federal do ABC ^b, São Paulo, Brazil

C.A. Bernardes^a, L. Calligaris^a, T.R. Fernandez Perez Tomei^a, E.M. Gregores^b, D.S. Lemos^a, P.G. Mercadante^b, S.F. Novaes^a, Sandra S. Padula^a

Institute for Nuclear Research and Nuclear Energy, Bulgarian Academy of Sciences, Sofia, Bulgaria

A. Aleksandrov, G. Antchev, R. Hadjiiska, P. Iaydjiev, M. Misheva, M. Rodozov, M. Shopova, G. Sultanov

University of Sofia, Sofia, Bulgaria

M. Bonchev, A. Dimitrov, T. Ivanov, L. Litov, B. Pavlov, P. Petkov, A. Petrov

Beihang University, Beijing, China
W. Fang², X. Gao², L. Yuan

Department of Physics, Tsinghua University, Beijing, China
M. Ahmad, Z. Hu, Y. Wang

Institute of High Energy Physics, Beijing, China
G.M. Chen⁸, H.S. Chen⁸, M. Chen, C.H. Jiang, D. Leggat, H. Liao, Z. Liu, A. Spiezia, J. Tao, E. Yazgan, H. Zhang, S. Zhang⁸, J. Zhao

State Key Laboratory of Nuclear Physics and Technology, Peking University, Beijing, China
A. Agapitos, Y. Ban, G. Chen, A. Levin, J. Li, L. Li, Q. Li, Y. Mao, S.J. Qian, D. Wang, Q. Wang

Zhejiang University, Hangzhou, China
M. Xiao

Universidad de Los Andes, Bogota, Colombia
C. Avila, A. Cabrera, C. Florez, C.F. González Hernández, M.A. Segura Delgado

Universidad de Antioquia, Medellin, Colombia
J. Mejia Guisao, J.D. Ruiz Alvarez, C.A. Salazar González, N. Vanegas Arbelaez

University of Split, Faculty of Electrical Engineering, Mechanical Engineering and Naval Architecture, Split, Croatia
D. Giljanović, N. Godinovic, D. Lelas, I. Puljak, T. Sculac

University of Split, Faculty of Science, Split, Croatia
Z. Antunovic, M. Kovac

Institute Rudjer Boskovic, Zagreb, Croatia
V. Brigljevic, D. Ferencek, K. Kadija, D. Majumder, B. Mesic, M. Roguljic, A. Starodumov⁹, T. Susa

University of Cyprus, Nicosia, Cyprus
M.W. Ather, A. Attikis, E. Erodotou, A. Ioannou, M. Kolosova, S. Konstantinou, G. Mavromanolakis, J. Mousa, C. Nicolaou, F. Ptochos, P.A. Razis, H. Rykaczewski, H. Saka, D. Tsiakkouri

Charles University, Prague, Czech Republic
M. Finger¹⁰, M. Finger Jr.¹⁰, A. Kveton, J. Tomsa

Escuela Politecnica Nacional, Quito, Ecuador
E. Ayala

Universidad San Francisco de Quito, Quito, Ecuador
E. Carrera Jarrin

Academy of Scientific Research and Technology of the Arab Republic of Egypt, Egyptian Network of High Energy Physics, Cairo, Egypt
S. Khalil¹¹

National Institute of Chemical Physics and Biophysics, Tallinn, Estonia
S. Bhowmik, A. Carvalho Antunes De Oliveira, R.K. Dewanjee, K. Ehataht, M. Kadastik, M. Raidal, C. Veelken

Department of Physics, University of Helsinki, Helsinki, Finland
P. Eerola, L. Forthomme, H. Kirschenmann, K. Osterberg, M. Voutilainen

Helsinki Institute of Physics, Helsinki, Finland

E. Brücken, F. Garcia, J. Havukainen, J.K. Heikkilä, V. Karimäki, M.S. Kim, R. Kinnunen, T. Lampén, K. Lassila-Perini, S. Laurila, S. Lehti, T. Lindén, H. Siikonen, E. Tuominen, J. Tuominiemi

Lappeenranta University of Technology, Lappeenranta, Finland

P. Luukka, T. Tuuva

IRFU, CEA, Université Paris-Saclay, Gif-sur-Yvette, France

M. Besancon, F. Couderc, M. Dejardin, D. Denegri, B. Fabbro, J.L. Faure, F. Ferri, S. Ganjour, A. Givernaud, P. Gras, G. Hamel de Monchenault, P. Jarry, C. Leloup, B. Lenzi, E. Locci, J. Malcles, J. Rander, A. Rosowsky, M.Ö. Sahin, A. Savoy-Navarro¹², M. Titov, G.B. Yu

Laboratoire Leprince-Ringuet, CNRS/IN2P3, Ecole Polytechnique, Institut Polytechnique de Paris, Paris, France

S. Ahuja, C. Amendola, F. Beaudette, M. Bonanomi, P. Busson, C. Charlot, B. Diab, G. Falmagne, R. Granier de Cassagnac, I. Kucher, A. Lobanov, C. Martin Perez, M. Nguyen, C. Ochando, P. Paganini, J. Rembser, R. Salerno, J.B. Sauvan, Y. Sirois, A. Zabi, A. Zghiche

Université de Strasbourg, CNRS, IPHC UMR 7178, Strasbourg, France

J.-L. Agram¹³, J. Andrea, D. Bloch, G. Bourgatte, J.-M. Brom, E.C. Chabert, C. Collard, E. Conte¹³, J.-C. Fontaine¹³, D. Gelé, U. Goerlach, C. Grimault, A.-C. Le Bihan, P. Van Hove

Centre de Calcul de l’Institut National de Physique Nucléaire et de Physique des Particules, CNRS/IN2P3, Villeurbanne, France

S. Gadrat

Université de Lyon, Université Claude Bernard Lyon 1, CNRS-IN2P3, Institut de Physique Nucléaire de Lyon, Villeurbanne, France

S. Beauceron, C. Bernet, G. Boudoul, C. Camen, A. Carle, N. Chanon, R. Chierici, D. Contardo, P. Depasse, H. El Mamouni, J. Fay, S. Gascon, M. Gouzevitch, B. Ille, Sa. Jain, I.B. Laktineh, H. Lattaud, A. Lesauvage, M. Lethuillier, L. Mirabito, S. Perries, V. Sordini, L. Torterotot, G. Touquet, M. Vander Donckt, S. Viret

Georgian Technical University, Tbilisi, Georgia

A. Khvedelidze¹⁰

Tbilisi State University, Tbilisi, Georgia

Z. Tsamalaidze¹⁰

RWTH Aachen University, I. Physikalisches Institut, Aachen, Germany

L. Feld, K. Klein, M. Lipinski, D. Meuser, A. Pauls, M. Preuten, M.P. Rauch, J. Schulz, M. Teroerde

RWTH Aachen University, III. Physikalisches Institut A, Aachen, Germany

M. Erdmann, B. Fischer, S. Ghosh, T. Hebbeker, K. Hoepfner, H. Keller, L. Mastrolorenzo, M. Merschmeyer, A. Meyer, P. Millet, G. Mocellin, S. Mondal, S. Mukherjee, D. Noll, A. Novak, T. Pook, A. Pozdnyakov, T. Quast, M. Radziej, Y. Rath, H. Reithler, J. Roemer, A. Schmidt, S.C. Schuler, A. Sharma, S. Wiedenbeck, S. Zaleski

RWTH Aachen University, III. Physikalisches Institut B, Aachen, Germany

G. Flügge, W. Haj Ahmad¹⁴, O. Hlushchenko, T. Kress, T. Müller, A. Nowack, C. Pistone, O. Pooth, D. Roy, H. Sert, A. Stahl¹⁵

Deutsches Elektronen-Synchrotron, Hamburg, Germany

H. Aarup Petersen, M. Aldaya Martin, P. Asmuss, I. Babounikau, K. Beernaert, O. Behnke, A. Bermúdez Martínez, A.A. Bin Anuar, K. Borras¹⁶, V. Botta, D. Brunner, A. Campbell, A. Cardini, P. Connor, S. Consuegra Rodríguez, C. Contreras-Campana, V. Danilov, A. De Wit, M.M. Defranchis, C. Diez Pardos, D. Domínguez Damiani, G. Eckerlin, D. Eckstein, T. Eichhorn, A. Elwood, E. Eren, L.I. Estevez Banos, E. Gallo¹⁷, A. Geiser, A. Grebenyuk, A. Grohsjean, M. Guthoff, M. Haranko, A. Harb, A. Jafari, N.Z. Jomhari, H. Jung, A. Kasem¹⁶, M. Kasemann, H. Kaveh, J. Keaveney, C. Kleinwort, J. Knolle, D. Krücker, W. Lange, T. Lenz, J. Lidrych, K. Lipka, W. Lohmann¹⁸, R. Mankel, I.-A. Melzer-Pellmann, J. Metwally, A.B. Meyer, M. Meyer, M. Missiroli, J. Mnich, A. Mussgiller, V. Myronenko, Y. Otarid, D. Pérez Adán, S.K. Pflitsch, D. Pitzl, A. Raspereza, A. Saibel, M. Savitskyi, V. Scheurer, P. Schütze, C. Schwanenberger, R. Shevchenko, A. Singh, R.E. Sosa Ricardo, H. Tholen, N. Tonon, O. Turkot, A. Vagnerini, M. Van De Klundert, R. Walsh, D. Walter, Y. Wen, K. Wichmann, C. Wissing, O. Zenaiev, R. Zlebcik

University of Hamburg, Hamburg, Germany

R. Aggleton, S. Bein, L. Benato, A. Benecke, K. De Leo, T. Dreyer, A. Ebrahimi, F. Feindt, A. Fröhlich, C. Garbers, E. Garutti, D. Gonzalez, P. Gunnellini, J. Haller, A. Hinzmann, A. Karavdina, G. Kasieczka, R. Klanner, R. Kogler, N. Kovalchuk, S. Kurz, V. Kutzner, J. Lange, T. Lange, A. Malara, J. Multhaup, C.E.N. Niemeyer, A. Reimers, O. Rieger, P. Schleper, S. Schumann, J. Schwandt, J. Sonneveld, H. Stadie, G. Steinbrück, B. Vormwald, I. Zoi

Karlsruher Institut fuer Technologie, Karlsruhe, Germany

M. Akbiyik, M. Baselga, S. Baur, T. Berger, E. Butz, R. Caspart, T. Chwalek, W. De Boer, A. Dierlamm, K. El Morabit, N. Faltermann, M. Giffels, A. Gottmann, F. Hartmann¹⁵, C. Heidecker, U. Husemann, M.A. Iqbal, S. Kudella, S. Maier, S. Mitra, M.U. Mozer, D. Müller, Th. Müller, M. Musich, A. Nürnberg, G. Quast, K. Rabbertz, D. Savoiu, D. Schäfer, M. Schnepf, M. Schröder, I. Shvetsov, H.J. Simonis, R. Ulrich, M. Wassmer, M. Weber, C. Wöhrmann, R. Wolf, S. Wozniewski

Institute of Nuclear and Particle Physics (INPP), NCSR Demokritos, Aghia Paraskevi, Greece

G. Anagnostou, P. Asenov, G. Daskalakis, T. Geralis, A. Kyriakis, D. Loukas, G. Paspalaki, A. Stakia

National and Kapodistrian University of Athens, Athens, Greece

M. Diamantopoulou, G. Karathanasis, P. Kontaxakis, A. Manousakis-katsikakis, A. Panagiotou, I. Papavergou, N. Saoulidou, K. Theofilatos, K. Vellidis, E. Vourliotis

National Technical University of Athens, Athens, Greece

G. Bakas, K. Kousouris, I. Papakrivopoulos, G. Tsipolitis, A. Zacharopoulou

University of Ioánnina, Ioánnina, Greece

I. Evangelou, C. Foudas, P. Gianneios, P. Katsoulis, P. Kokkas, S. Mallios, K. Manitara, N. Manthos, I. Papadopoulos, J. Strologas, F.A. Triantis, D. Tsitsonis

MTA-ELTE Lendület CMS Particle and Nuclear Physics Group, Eötvös Loránd University, Budapest, Hungary

M. Bartók¹⁹, R. Chudasama, M. Csanad, M.M.A. Gadallah, P. Major, K. Mandal, A. Mehta, G. Pasztor, O. Surányi, G.I. Veres

Wigner Research Centre for Physics, Budapest, Hungary

G. Bencze, C. Hajdu, D. Horvath²⁰, F. Sikler, V. Veszpremi, G. Vesztregombi[†]

Institute of Nuclear Research ATOMKI, Debrecen, Hungary

N. Beni, S. Czellar, J. Karancsi¹⁹, J. Molnar, Z. Szillasi, D. Teyssier

Institute of Physics, University of Debrecen, Debrecen, Hungary

P. Raics, Z.L. Trocsanyi, B. Ujvari

Eszterhazy Karoly University, Karoly Robert Campus, Gyongyos, Hungary

T. Csorgo, S. Lökös, W.J. Metzger, F. Nemes, T. Novak

Indian Institute of Science (IISc), Bangalore, India

S. Choudhury, J.R. Komaragiri, L. Panwar, P.C. Tiwari

National Institute of Science Education and Research, HBNI, Bhubaneswar, India

S. Bahinipati²², C. Kar, G. Kole, P. Mal, V.K. Muraleedharan Nair Bindhu, A. Nayak²³, D.K. Sahoo²², N. Sur, S.K. Swain

Punjab University, Chandigarh, India

S. Bansal, S.B. Beri, V. Bhatnagar, S. Chauhan, N. Dhingra²⁴, R. Gupta, A. Kaur, A. Kaur, M. Kaur, S. Kaur, P. Kumari, M. Lohan, M. Meena, K. Sandeep, S. Sharma, J.B. Singh, A.K. Virdi

University of Delhi, Delhi, India

A. Ahmed, A. Bhardwaj, B.C. Choudhary, R.B. Garg, M. Gola, S. Keshri, A. Kumar, M. Naimuddin, P. Priyanka, K. Ranjan, A. Shah, R. Sharma

Saha Institute of Nuclear Physics, HBNI, Kolkata, India

R. Bhardwaj²⁵, M. Bharti²⁵, R. Bhattacharya, S. Bhattacharya, U. Bhawandeep²⁵, D. Bhowmik, S. Dutta, S. Ghosh, B. Gomber²⁶, M. Maity²⁷, K. Mondal, S. Nandan, P. Palit, A. Purohit, P.K. Rout, G. Saha, S. Sarkar, M. Sharan, B. Singh²⁵, S. Thakur²⁵

Indian Institute of Technology Madras, Madras, India

P.K. Behera, S.C. Behera, P. Kalbhor, A. Muhammad, R. Pradhan, P.R. Pujahari, A. Sharma, A.K. Sikdar

Bhabha Atomic Research Centre, Mumbai, India

D. Dutta, V. Jha, D.K. Mishra, P.K. Netrakanti, L.M. Pant, P. Shukla

Tata Institute of Fundamental Research-A, Mumbai, India

T. Aziz, M.A. Bhat, S. Dugad, R. Kumar Verma, G.B. Mohanty, U. Sarkar

Tata Institute of Fundamental Research-B, Mumbai, India

S. Banerjee, S. Bhattacharya, S. Chatterjee, P. Das, M. Guchait, S. Karmakar, S. Kumar, G. Majumder, K. Mazumdar, N. Sahoo, S. Sawant

Indian Institute of Science Education and Research (IISER), Pune, India

S. Dube, B. Kansal, A. Kapoor, K. Kotheendar, S. Pandey, A. Rane, A. Rastogi, S. Sharma

Department of Physics, Isfahan University of Technology, Isfahan, Iran

H. Bakhshiansohi

Institute for Research in Fundamental Sciences (IPM), Tehran, Iran

S. Chenarani, S.M. Etesami, M. Khakzad, M. Mohammadi Najafabadi, M. Naseri, F. Rezaei Hosseiniabadi

University College Dublin, Dublin, Ireland

M. Felcini, M. Grunewald

INFN Sezione di Bari ^a, Università di Bari ^b, Politecnico di Bari ^c, Bari, Italy

M. Abbrescia^{a,b}, R. Aly^{a,b,28}, C. Calabria^{a,b}, A. Colaleo^a, D. Creanza^{a,c}, L. Cristella^{a,b}, N. De Filippis^{a,c}, M. De Palma^{a,b}, A. Di Florio^{a,b}, W. Elmetenawee^{a,b}, L. Fiore^a, A. Gelmi^{a,b}, G. Iaselli^{a,c}, M. Ince^{a,b}, S. Lezki^{a,b}, G. Maggi^{a,c}, M. Maggi^a, J.A. Merlin^a, G. Miniello^{a,b}, S. My^{a,b}, S. Nuzzo^{a,b}, A. Pompili^{a,b}, G. Pugliese^{a,c}, R. Radogna^a, A. Ranieri^a, G. Selvaggi^{a,b}, L. Silvestris^a, F.M. Simone^{a,b}, R. Venditti^a, P. Verwilligen^a

INFN Sezione di Bologna ^a, Università di Bologna ^b, Bologna, Italy

G. Abbiendi^a, C. Battilana^{a,b}, D. Bonacorsia^{a,b}, L. Borgonovi^{a,b}, S. Braibant-Giacomelli^{a,b}, R. Campanini^{a,b}, P. Capiluppi^{a,b}, A. Castro^{a,b}, F.R. Cavallo^a, C. Ciocca^a, G. Codispoti^{a,b}, M. Cuffiani^{a,b}, G.M. Dallavalle^a, F. Fabbri^a, A. Fanfani^{a,b}, E. Fontanesi^{a,b}, P. Giacomelli^a, C. Grandi^a, L. Guiducci^{a,b}, F. Iemmi^{a,b}, S. Lo Meo^{a,29}, S. Marcellini^a, G. Masetti^a, F.L. Navarria^{a,b}, A. Perrotta^a, F. Primavera^{a,b}, A.M. Rossi^{a,b}, T. Rovelli^{a,b}, G.P. Siroli^{a,b}, N. Tosi^a

INFN Sezione di Catania ^a, Università di Catania ^b, Catania, Italy

S. Albergo^{a,b,30}, S. Costa^{a,b}, A. Di Mattia^a, R. Potenza^{a,b}, A. Tricomi^{a,b,30}, C. Tuve^{a,b}

INFN Sezione di Firenze ^a, Università di Firenze ^b, Firenze, Italy

G. Barbagli^a, A. Cassese^a, R. Ceccarelli^{a,b}, V. Ciulli^{a,b}, C. Civinini^a, R. D'Alessandro^{a,b}, F. Fiori^a, E. Focardi^{a,b}, G. Latino^{a,b}, P. Lenzi^{a,b}, M. Lizzo^{a,b}, M. Meschini^a, S. Paoletti^a, R. Seidita^{a,b}, G. Sguazzoni^a, L. Viliani^a

INFN Laboratori Nazionali di Frascati, Frascati, Italy

L. Benussi, S. Bianco, D. Piccolo

INFN Sezione di Genova ^a, Università di Genova ^b, Genova, Italy

M. Bozzo^{a,b}, F. Ferro^a, R. Mulargia^{a,b}, E. Robutti^a, S. Tosi^{a,b}

INFN Sezione di Milano-Bicocca ^a, Università di Milano-Bicocca ^b, Milano, Italy

A. Benaglia^a, A. Beschi^{a,b}, F. Brivio^{a,b}, V. Ciriolo^{a,b,15}, F. De Guio^{a,b}, M.E. Dinardo^{a,b}, P. Dini^a, S. Gennai^a, A. Ghezzi^{a,b}, P. Govoni^{a,b}, L. Guzzi^{a,b}, M. Malberti^a, S. Malvezzi^a, D. Menasce^a, F. Monti^{a,b}, L. Moroni^a, M. Paganoni^{a,b}, D. Pedrini^a, S. Ragazzi^{a,b}, T. Tabarelli de Fatis^{a,b}, D. Valsecchi^{a,b,15}, D. Zuolo^{a,b}

INFN Sezione di Napoli ^a, Università di Napoli 'Federico II' ^b, Napoli, Italy, Università della Basilicata ^c, Potenza, Italy, Università G. Marconi ^d, Roma, Italy

S. Buontempo^a, N. Cavallo^{a,c}, A. De Iorio^{a,b}, A. Di Crescenzo^{a,b}, F. Fabozzi^{a,c}, F. Fienga^a, G. Galati^a, A.O.M. Iorio^{a,b}, L. Layer^{a,b}, L. Lista^{a,b}, S. Meola^{a,d,15}, P. Paolucci^{a,15}, B. Rossi^a, C. Sciacca^{a,b}, E. Voevodina^{a,b}

INFN Sezione di Padova ^a, Università di Padova ^b, Padova, Italy, Università di Trento ^c, Trento, Italy

P. Azzi^a, N. Bacchetta^a, D. Bisello^{a,b}, A. Boletti^{a,b}, A. Bragagnolo^{a,b}, R. Carlin^{a,b}, P. Checchia^a, P. De Castro Manzano^a, T. Dorigo^a, U. Dosselli^a, F. Gasparini^{a,b}, U. Gasparini^{a,b}, A. Gozzelino^a, S.Y. Hoh^{a,b}, M. Margoni^{a,b}, A.T. Meneguzzo^{a,b}, J. Pazzini^{a,b}, M. Presilla^b, P. Ronchese^{a,b}, R. Rossin^{a,b}, F. Simonetto^{a,b}, A. Tiko^a, M. Tosi^{a,b}, H. YARAR^{a,b}, M. Zanetti^{a,b}, P. Zotto^{a,b}, A. Zucchetta^{a,b}

INFN Sezione di Pavia ^a, Università di Pavia ^b, Pavia, Italy

A. Braghieri^a, S. Calzaferri^{a,b}, D. Fiorina^{a,b}, P. Montagna^{a,b}, S.P. Ratti^{a,b}, V. Re^a, M. Ressegotti^{a,b}, C. Riccardi^{a,b}, P. Salvini^a, I. Vai^a, P. Vitulo^{a,b}

INFN Sezione di Perugia ^a, Università di Perugia ^b, Perugia, Italy

M. Biasini^{a,b}, G.M. Bilei^a, D. Ciangottini^{a,b}, L. Fanò^{a,b}, P. Lariccia^{a,b}, R. Leonardi^{a,b}, E. Manoni^a, G. Mantovani^{a,b}, V. Mariani^{a,b}, M. Menichelli^a, A. Rossi^{a,b}, A. Santocchia^{a,b}, D. Spiga^a

INFN Sezione di Pisa ^a, Università di Pisa ^b, Scuola Normale Superiore di Pisa ^c, Pisa, Italy
 K. Androsov^a, P. Azzurri^a, G. Bagliesi^a, V. Bertacchi^{a,c}, L. Bianchini^a, T. Boccali^a, R. Castaldi^a, M.A. Ciocci^{a,b}, R. Dell'Orso^a, S. Donato^a, L. Giannini^{a,c}, A. Giassi^a, M.T. Grippo^a, F. Ligabue^{a,c}, E. Manca^{a,c}, G. Mandorli^{a,c}, A. Messineo^{a,b}, F. Palla^a, A. Rizzi^{a,b}, G. Rolandi^{a,c}, S. Roy Chowdhury^{a,c}, A. Scribano^a, P. Spagnolo^a, R. Tenchini^a, G. Tonelli^{a,b}, N. Turini^a, A. Venturi^a, P.G. Verdini^a

INFN Sezione di Roma ^a, Sapienza Università di Roma ^b, Rome, Italy

F. Cavallari^a, M. Cipriani^{a,b}, D. Del Re^{a,b}, E. Di Marco^a, M. Diemoz^a, E. Longo^{a,b}, P. Meridiani^a, G. Organtini^{a,b}, F. Pandolfi^a, R. Paramatti^{a,b}, C. Quaranta^{a,b}, S. Rahatlou^{a,b}, C. Rovelli^a, F. Santanastasio^{a,b}, L. Soffi^{a,b}, R. Tramontano^{a,b}

INFN Sezione di Torino ^a, Università di Torino ^b, Torino, Italy, Università del Piemonte Orientale ^c, Novara, Italy

N. Amapane^{a,b}, R. Arcidiacono^{a,c}, S. Argiro^{a,b}, M. Arneodo^{a,c}, N. Bartosik^a, R. Bellan^{a,b}, A. Bellora^{a,b}, C. Biino^a, A. Cappati^{a,b}, N. Cartiglia^a, S. Cometti^a, M. Costa^{a,b}, R. Covarelli^{a,b}, N. Demaria^a, J.R. González Fernández^a, B. Kiani^{a,b}, F. Legger^a, C. Mariotti^a, S. Maselli^a, E. Migliore^{a,b}, V. Monaco^{a,b}, E. Monteil^{a,b}, M. Monteno^a, M.M. Obertino^{a,b}, G. Ortona^a, L. Pacher^{a,b}, N. Pastrone^a, M. Pelliccioni^a, G.L. Pinna Angioni^{a,b}, M. Ruspa^{a,c}, R. Salvatico^{a,b}, F. Siviero^{a,b}, V. Sola^a, A. Solano^{a,b}, D. Soldi^{a,b}, A. Staiano^a, D. Trocino^{a,b}

INFN Sezione di Trieste ^a, Università di Trieste ^b, Trieste, Italy

S. Belforte^a, V. Candelise^{a,b}, M. Casarsa^a, F. Cossutti^a, A. Da Rold^{a,b}, G. Della Ricca^{a,b}, F. Vazzoler^{a,b}, A. Zanetti^a

Kyungpook National University, Daegu, Korea

B. Kim, D.H. Kim, G.N. Kim, J. Lee, S.W. Lee, C.S. Moon, Y.D. Oh, S.I. Pak, S. Sekmen, D.C. Son, Y.C. Yang

Chonnam National University, Institute for Universe and Elementary Particles, Kwangju, Korea

H. Kim, D.H. Moon

Hanyang University, Seoul, Korea

B. Francois, T.J. Kim, J. Park

Korea University, Seoul, Korea

S. Cho, S. Choi, Y. Go, S. Ha, B. Hong, K. Lee, K.S. Lee, J. Lim, J. Park, S.K. Park, Y. Roh, J. Yoo

Kyung Hee University, Department of Physics, Seoul, Republic of Korea

J. Goh

Sejong University, Seoul, Korea

H.S. Kim

Seoul National University, Seoul, Korea

J. Almond, J.H. Bhyun, J. Choi, S. Jeon, J. Kim, J.S. Kim, S. Ko, H. Lee, K. Lee, S. Lee, K. Nam, B.H. Oh, M. Oh, S.B. Oh, B.C. Radburn-Smith, H. Seo, U.K. Yang, H.D. Yoo, I. Yoon

University of Seoul, Seoul, Korea

D. Jeon, J.H. Kim, J.S.H. Lee, I.C. Park, I.J. Watson

Sungkyunkwan University, Suwon, Korea

Y. Choi, C. Hwang, Y. Jeong, J. Lee, Y. Lee, I. Yu

Riga Technical University, Riga, Latvia

V. Veckalns³¹

Vilnius University, Vilnius, Lithuania

V. Dudenė, A. Juodagalvis, A. Rinkevičius, G. Tamulaitis, J. Vaitkus

National Centre for Particle Physics, Universiti Malaya, Kuala Lumpur, Malaysia

F. Mohamad Idris³², W.A.T. Wan Abdullah, M.N. Yusli, Z. Zolkapli

Universidad de Sonora (UNISON), Hermosillo, Mexico

J.F. Benitez, A. Castaneda Hernandez, J.A. Murillo Quijada, L. Valencia Palomo

Centro de Investigacion y de Estudios Avanzados del IPN, Mexico City, Mexico

H. Castilla-Valdez, E. De La Cruz-Burelo, I. Heredia-De La Cruz³³, R. Lopez-Fernandez, A. Sanchez-Hernandez

Universidad Iberoamericana, Mexico City, Mexico

S. Carrillo Moreno, C. Oropeza Barrera, M. Ramirez-Garcia, F. Vazquez Valencia

Benemerita Universidad Autonoma de Puebla, Puebla, Mexico

J. Eysermans, I. Pedraza, H.A. Salazar Ibarguen, C. Uribe Estrada

Universidad Autónoma de San Luis Potosí, San Luis Potosí, Mexico

A. Morelos Pineda

University of Montenegro, Podgorica, Montenegro

J. Mijuskovic³, N. Raicevic

University of Auckland, Auckland, New Zealand

D. Kofcheck

University of Canterbury, Christchurch, New Zealand

S. Bheesette, P.H. Butler, P. Lujan

National Centre for Physics, Quaid-I-Azam University, Islamabad, Pakistan

A. Ahmad, M. Ahmad, M.I.M. Awan, Q. Hassan, H.R. Hoorani, W.A. Khan, M.A. Shah, M. Shoaib, M. Waqas

AGH University of Science and Technology Faculty of Computer Science, Electronics and Telecommunications, Krakow, Poland

V. Avati, L. Grzanka, M. Malawski

National Centre for Nuclear Research, Swierk, Poland

H. Bialkowska, M. Bluj, B. Boimska, M. Górski, M. Kazana, M. Szleper, P. Zalewski

Institute of Experimental Physics, Faculty of Physics, University of Warsaw, Warsaw, Poland

K. Bunkowski, A. Byszuk³⁴, K. Doroba, A. Kalinowski, M. Konecki, J. Krolikowski, M. Olszewski, M. Walczak

Laboratório de Instrumentação e Física Experimental de Partículas, Lisboa, Portugal

M. Araujo, P. Bargassa, D. Bastos, A. Di Francesco, P. Faccioli, B. Galinhas, M. Gallinaro, J. Hollar, N. Leonardo, T. Niknejad, J. Seixas, K. Shchelina, G. Strong, O. Toldaiev, J. Varela

Joint Institute for Nuclear Research, Dubna, Russia

S. Afanasiev, P. Bunin, M. Gavrilenko, I. Golutvin, I. Gorbunov, A. Kamenev, V. Karjavine,

V. Korenkov, A. Lanev, A. Malakhov, V. Matveev^{35,36}, P. Moisenz, V. Palichik, V. Perelygin, M. Savina, S. Shmatov, N. Skatchkov, V. Smirnov, B.S. Yuldashev³⁷, A. Zarubin

Petersburg Nuclear Physics Institute, Gatchina (St. Petersburg), Russia

L. Chtchipounov, V. Golovtcov, Y. Ivanov, V. Kim³⁸, E. Kuznetsova³⁹, P. Levchenko, V. Murzin, V. Oreshkin, I. Smirnov, D. Sosnov, V. Sulimov, L. Uvarov, A. Vorobyev

Institute for Nuclear Research, Moscow, Russia

Yu. Andreev, A. Dermenev, S. Glinenko, N. Golubev, A. Karneyeu, M. Kirsanov, N. Krasnikov, A. Pashenkov, D. Tlisov, A. Toropin

Institute for Theoretical and Experimental Physics named by A.I. Alikhanov of NRC 'Kurchatov Institute', Moscow, Russia

V. Epshteyn, V. Gavrilov, N. Lychkovskaya, A. Nikitenko⁴⁰, V. Popov, I. Pozdnyakov, G. Safronov, A. Spiridonov, A. Stepenov, M. Toms, E. Vlasov, A. Zhokin

Moscow Institute of Physics and Technology, Moscow, Russia

T. Aushev

National Research Nuclear University 'Moscow Engineering Physics Institute' (MEPhI), Moscow, Russia

M. Chadeeva⁴¹, A. Osokin, P. Parygin, E. Popova, V. Rusinov

P.N. Lebedev Physical Institute, Moscow, Russia

V. Andreev, M. Azarkin, I. Dremin, M. Kirakosyan, A. Terkulov

Skobeltsyn Institute of Nuclear Physics, Lomonosov Moscow State University, Moscow, Russia

A. Baskakov, A. Belyaev, E. Boos, V. Bunichev, M. Dubinin⁴², L. Dudko, V. Klyukhin, O. Kodolova, I. Lokhtin, S. Obraztsov, M. Perfilov, S. Petrushanko, V. Savrin

Novosibirsk State University (NSU), Novosibirsk, Russia

V. Blinov⁴³, T. Dimova⁴³, L. Kardapoltsev⁴³, I. Ovtin⁴³, Y. Skovpen⁴³

Institute for High Energy Physics of National Research Centre 'Kurchatov Institute', Protvino, Russia

I. Azhgirey, I. Bayshev, S. Bitioukov, V. Kachanov, D. Konstantinov, P. Mandrik, V. Petrov, R. Ryutin, S. Slabospitskii, A. Sobol, S. Troshin, N. Tyurin, A. Uzunian, A. Volkov

National Research Tomsk Polytechnic University, Tomsk, Russia

A. Babaev, A. Iuzhakov, V. Okhotnikov

Tomsk State University, Tomsk, Russia

V. Borchsh, V. Ivanchenko, E. Tcherniaev

University of Belgrade: Faculty of Physics and VINCA Institute of Nuclear Sciences, Belgrade, Serbia

P. Adzic⁴⁴, P. Cirkovic, M. Dordevic, P. Milenovic, J. Milosevic, M. Stojanovic

Centro de Investigaciones Energéticas Medioambientales y Tecnológicas (CIEMAT), Madrid, Spain

M. Aguilar-Benitez, J. Alcaraz Maestre, A. Álvarez Fernández, I. Bachiller, M. Barrio Luna, Cristina F. Bedoya, J.A. Brochero Cifuentes, C.A. Carrillo Montoya, M. Cepeda, M. Cerrada, N. Colino, B. De La Cruz, A. Delgado Peris, J.P. Fernández Ramos, J. Flix, M.C. Fouz, O. Gonzalez Lopez, S. Goy Lopez, J.M. Hernandez, M.I. Josa, D. Moran, Á. Navarro Tobar,

A. Pérez-Calero Yzquierdo, J. Puerta Pelayo, I. Redondo, L. Romero, S. Sánchez Navas, M.S. Soares, A. Triossi, C. Willmott

Universidad Autónoma de Madrid, Madrid, Spain

C. Albajar, J.F. de Trocóniz, R. Reyes-Almanza

Universidad de Oviedo, Instituto Universitario de Ciencias y Tecnologías Espaciales de Asturias (ICTEA), Oviedo, Spain

B. Alvarez Gonzalez, J. Cuevas, C. Erice, J. Fernandez Menendez, S. Folgueras, I. Gonzalez Caballero, E. Palencia Cortezon, C. Ramón Álvarez, V. Rodríguez Bouza, S. Sanchez Cruz

Instituto de Física de Cantabria (IFCA), CSIC-Universidad de Cantabria, Santander, Spain

I.J. Cabrillo, A. Calderon, B. Chazin Quero, J. Duarte Campderros, M. Fernandez, P.J. Fernández Manteca, A. García Alonso, G. Gomez, C. Martinez Rivero, P. Martinez Ruiz del Arbol, F. Matorras, J. Piedra Gomez, C. Prieels, F. Ricci-Tam, T. Rodrigo, A. Ruiz-Jimeno, L. Russo⁴⁵, L. Scodellaro, I. Vila, J.M. Vizan Garcia

University of Colombo, Colombo, Sri Lanka

D.U.J. Sonnadara

University of Ruhuna, Department of Physics, Matara, Sri Lanka

W.G.D. Dharmaratna, N. Wickramage

CERN, European Organization for Nuclear Research, Geneva, Switzerland

T.K. Arrestad, D. Abbaneo, B. Akgun, E. Auffray, G. Auzinger, J. Baechler, P. Baillon, A.H. Ball, D. Barney, J. Bendavid, M. Bianco, A. Bocci, P. Bortignon, E. Bossini, E. Brondolin, T. Camporesi, A. Caratelli, G. Cerminara, E. Chapon, G. Cucciati, D. d'Enterria, A. Dabrowski, N. Daci, V. Daponte, A. David, O. Davignon, A. De Roeck, M. Deile, R. Di Maria, M. Dobson, M. Dünser, N. Dupont, A. Elliott-Peisert, N. Emriskova, F. Fallavollita⁴⁶, D. Fasanella, S. Fiorendi, G. Franzoni, J. Fulcher, W. Funk, S. Giani, D. Gigi, K. Gill, F. Gleje, L. Gouskos, M. Gruchala, M. Guilbaud, D. Gulhan, J. Hegeman, C. Heidegger, Y. Iiyama, V. Innocente, T. James, P. Janot, O. Karacheban¹⁸, J. Kaspar, J. Kieseler, M. Krammer¹, N. Kratochwil, C. Lange, P. Lecoq, K. Long, C. Lourenço, L. Malgeri, M. Mannelli, A. Massironi, F. Meijers, S. Mersi, E. Meschi, F. Moortgat, M. Mulders, J. Ngadiuba, J. Niedziela, S. Nourbakhsh, S. Orfanelli, L. Orsini, F. Pantaleo¹⁵, L. Pape, E. Perez, M. Peruzzi, A. Petrilli, G. Petrucciani, A. Pfeiffer, M. Pierini, F.M. Pitters, D. Rabady, A. Racz, M. Rieger, M. Rovere, H. Sakulin, J. Salfeld-Nebgen, S. Scarfi, C. Schäfer, C. Schwick, M. Selvaggi, A. Sharma, P. Silva, W. Snoeys, P. Sphicas⁴⁷, J. Steggemann, S. Summers, V.R. Tavolaro, D. Treille, A. Tsirou, G.P. Van Onsem, A. Vartak, M. Verzetti, K.A. Wozniak, W.D. Zeuner

Paul Scherrer Institut, Villigen, Switzerland

L. Caminada⁴⁸, K. Deiters, W. Erdmann, R. Horisberger, Q. Ingram, H.C. Kaestli, D. Kotlinski, U. Langenegger, T. Rohe

ETH Zurich - Institute for Particle Physics and Astrophysics (IPA), Zurich, Switzerland

M. Backhaus, P. Berger, A. Calandri, N. Chernyavskaya, G. Dissertori, M. Dittmar, M. Donegà, C. Dorfer, T. Gadek, T.A. Gómez Espinosa, C. Grab, D. Hits, W. Lustermann, R.A. Manzoni, M.T. Meinhard, F. Micheli, P. Musella, F. Nessi-Tedaldi, F. Pauss, V. Perovic, G. Perrin, L. Perrozzi, S. Pigazzini, M.G. Ratti, M. Reichmann, C. Reissel, T. Reitenspiess, B. Ristic, D. Ruini, D.A. Sanz Becerra, M. Schönenberger, L. Shchutska, M.L. Vesterbacka Olsson, R. Wallny, D.H. Zhu

Universität Zürich, Zurich, Switzerland

C. Amsler⁴⁹, C. Botta, D. Brzhechko, M.F. Canelli, A. De Cosa, R. Del Burgo, B. Kilminster,

S. Leontsinis, V.M. Mikuni, I. Neutelings, G. Rauco, P. Robmann, K. Schweiger, Y. Takahashi, S. Wertz

National Central University, Chung-Li, Taiwan

C.M. Kuo, W. Lin, A. Roy, T. Sarkar²⁷, S.S. Yu

National Taiwan University (NTU), Taipei, Taiwan

P. Chang, Y. Chao, K.F. Chen, P.H. Chen, W.-S. Hou, Y.y. Li, R.-S. Lu, E. Paganis, A. Psallidas, A. Steen

Chulalongkorn University, Faculty of Science, Department of Physics, Bangkok, Thailand

B. Asavapibhop, C. Asawatangtrakuldee, N. Srimanobhas, N. Suwonjandee

Çukurova University, Physics Department, Science and Art Faculty, Adana, Turkey

A. Bat, F. Boran, A. Celik⁵⁰, S. Damarseckin⁵¹, Z.S. Demiroglu, F. Dolek, C. Dozen⁵², I. Dumanoglu⁵³, G. Gokbulut, Y. Guler, E. Gurpinar Guler⁵⁴, I. Hos⁵⁵, C. Isik, E.E. Kangal⁵⁶, O. Kara, A. Kayis Topaksu, U. Kiminsu, G. Onengut, K. Ozdemir⁵⁷, A.E. Simsek, U.G. Tok, S. Turkcapar, I.S. Zorbakir, C. Zorbilmez

Middle East Technical University, Physics Department, Ankara, Turkey

B. Isildak⁵⁸, G. Karapinar⁵⁹, M. Yalvac⁶⁰

Bogazici University, Istanbul, Turkey

I.O. Atakisi, E. Gülmез, M. Kaya⁶¹, O. Kaya⁶², Ö. Özçelik, S. Tekten⁶³, E.A. Yetkin⁶⁴

Istanbul Technical University, Istanbul, Turkey

A. Cakir, K. Cankocak⁵³, Y. Komurcu, S. Sen⁶⁵

Istanbul University, Istanbul, Turkey

S. Cerci⁶⁶, B. Kaynak, S. Ozkorucuklu, D. Sunar Cerci⁶⁶

Institute for Scintillation Materials of National Academy of Science of Ukraine, Kharkov, Ukraine

B. Grynyov

National Scientific Center, Kharkov Institute of Physics and Technology, Kharkov, Ukraine

L. Levchuk

University of Bristol, Bristol, United Kingdom

E. Bhal, S. Bologna, J.J. Brooke, D. Burns⁶⁷, E. Clement, D. Cussans, H. Flacher, J. Goldstein, G.P. Heath, H.F. Heath, L. Kreczko, B. Krikler, S. Paramesvaran, T. Sakuma, S. Seif El Nasr-Storey, V.J. Smith, J. Taylor, A. Titterton

Rutherford Appleton Laboratory, Didcot, United Kingdom

K.W. Bell, A. Belyaev⁶⁸, C. Brew, R.M. Brown, D.J.A. Cockerill, J.A. Coughlan, K. Harder, S. Harper, J. Linacre, K. Manolopoulos, D.M. Newbold, E. Olaiya, D. Petyt, T. Reis, T. Schuh, C.H. Shepherd-Themistocleous, A. Thea, I.R. Tomalin, T. Williams

Imperial College, London, United Kingdom

R. Bainbridge, P. Bloch, S. Bonomally, J. Borg, S. Breeze, O. Buchmuller, A. Bundock, G.S. Chahal⁶⁹, D. Colling, P. Dauncey, G. Davies, M. Della Negra, P. Everaerts, G. Hall, G. Iles, M. Komm, J. Langford, L. Lyons, A.-M. Magnan, S. Malik, A. Martelli, V. Milosevic, A. Morton, J. Nash⁷⁰, V. Palladino, M. Pesaresi, D.M. Raymond, A. Richards, A. Rose, E. Scott, C. Seez, A. Shtipliyski, M. Stoye, A. Tapper, K. Uchida, T. Virdee¹⁵, N. Wardle, S.N. Webb, D. Winterbottom, A.G. Zecchinelli, S.C. Zenz

Brunel University, Uxbridge, United Kingdom

J.E. Cole, P.R. Hobson, A. Khan, P. Kyberd, C.K. Mackay, I.D. Reid, L. Teodorescu, S. Zahid

Baylor University, Waco, USA

A. Brinkerhoff, K. Call, B. Caraway, J. Dittmann, K. Hatakeyama, C. Madrid, B. McMaster, N. Pastika, C. Smith

Catholic University of America, Washington, DC, USA

R. Bartek, A. Dominguez, R. Uniyal, A.M. Vargas Hernandez

The University of Alabama, Tuscaloosa, USA

A. Buccilli, S.I. Cooper, S.V. Gleyzer, C. Henderson, P. Rumerio, C. West

Boston University, Boston, USA

A. Albert, D. Arcaro, Z. Demiragli, D. Gastler, C. Richardson, J. Rohlf, D. Sperka, D. Spitzbart, I. Suarez, L. Sulak, D. Zou

Brown University, Providence, USA

G. Benelli, B. Burkle, X. Coubez¹⁶, D. Cutts, Y.t. Duh, M. Hadley, U. Heintz, J.M. Hogan⁷¹, K.H.M. Kwok, E. Laird, G. Landsberg, K.T. Lau, J. Lee, M. Narain, S. Sagir⁷², R. Syarif, E. Usai, W.Y. Wong, D. Yu, W. Zhang

University of California, Davis, Davis, USA

R. Band, C. Brainerd, R. Breedon, M. Calderon De La Barca Sanchez, M. Chertok, J. Conway, R. Conway, P.T. Cox, R. Erbacher, C. Flores, G. Funk, F. Jensen, W. Ko[†], O. Kukral, R. Lander, M. Mulhearn, D. Pellett, J. Pilot, M. Shi, D. Taylor, K. Tos, M. Tripathi, Z. Wang, Y. Yao, F. Zhang

University of California, Los Angeles, USA

M. Bachtis, C. Bravo, R. Cousins, A. Dasgupta, A. Florent, J. Hauser, M. Ignatenko, N. Mccoll, W.A. Nash, S. Regnard, D. Saltzberg, C. Schnable, B. Stone, V. Valuev

University of California, Riverside, Riverside, USA

K. Burt, Y. Chen, R. Clare, J.W. Gary, S.M.A. Ghiasi Shirazi, G. Hanson, G. Karapostoli, O.R. Long, N. Manganelli, M. Olmedo Negrete, M.I. Paneva, W. Si, S. Wimpenny, Y. Zhang

University of California, San Diego, La Jolla, USA

J.G. Branson, P. Chang, S. Cittolin, S. Cooperstein, N. Deelen, M. Derdzinski, J. Duarte, R. Gerosa, D. Gilbert, B. Hashemi, D. Klein, V. Krutelyov, J. Letts, M. Masciovecchio, S. May, S. Padhi, M. Pieri, V. Sharma, M. Tadel, F. Würthwein, A. Yagil, G. Zevi Della Porta

University of California, Santa Barbara - Department of Physics, Santa Barbara, USA

N. Amin, R. Bhandari, C. Campagnari, M. Citron, V. Dutta, J. Incandela, B. Marsh, H. Mei, A. Ovcharova, H. Qu, J. Richman, U. Sarica, D. Stuart, S. Wang

California Institute of Technology, Pasadena, USA

D. Anderson, A. Bornheim, O. Cerri, I. Dutta, J.M. Lawhorn, N. Lu, J. Mao, H.B. Newman, T.Q. Nguyen, J. Pata, M. Spiropulu, J.R. Vlimant, S. Xie, Z. Zhang, R.Y. Zhu

Carnegie Mellon University, Pittsburgh, USA

J. Alison, M.B. Andrews, T. Ferguson, T. Mudholkar, M. Paulini, M. Sun, I. Vorobiev, M. Weinberg

University of Colorado Boulder, Boulder, USA

J.P. Cumalat, W.T. Ford, E. MacDonald, T. Mulholland, R. Patel, A. Perloff, K. Stenson, K.A. Ulmer, S.R. Wagner

Cornell University, Ithaca, USA

J. Alexander, Y. Cheng, J. Chu, A. Datta, A. Frankenthal, K. Mcdermott, J.R. Patterson, D. Quach, A. Ryd, S.M. Tan, Z. Tao, J. Thom, P. Wittich, M. Zientek

Fermi National Accelerator Laboratory, Batavia, USA

S. Abdullin, M. Albrow, M. Alyari, G. Apollinari, A. Apresyan, A. Apyan, S. Banerjee, L.A.T. Bauerdick, A. Beretvas, D. Berry, J. Berryhill, P.C. Bhat, K. Burkett, J.N. Butler, A. Canepa, G.B. Cerati, H.W.K. Cheung, F. Chlebana, M. Cremonesi, V.D. Elvira, J. Freeman, Z. Gecse, E. Gottschalk, L. Gray, D. Green, S. Grünendahl, O. Gutsche, R.M. Harris, S. Hasegawa, R. Heller, J. Hirschauer, B. Jayatilaka, S. Jindariani, M. Johnson, U. Joshi, T. Klijnsma, B. Klima, M.J. Kortelainen, B. Kreis, S. Lammel, J. Lewis, D. Lincoln, R. Lipton, M. Liu, T. Liu, J. Lykken, K. Maeshima, J.M. Marraffino, D. Mason, P. McBride, P. Merkel, S. Mrenna, S. Nahn, V. O'Dell, V. Papadimitriou, K. Pedro, C. Pena⁴², F. Ravera, A. Reinsvold Hall, L. Ristori, B. Schneider, E. Sexton-Kennedy, N. Smith, A. Soha, W.J. Spalding, L. Spiegel, S. Stoynev, J. Strait, L. Taylor, S. Tkaczyk, N.V. Tran, L. Uplegger, E.W. Vaandering, R. Vidal, M. Wang, H.A. Weber, A. Woodard

University of Florida, Gainesville, USA

D. Acosta, P. Avery, D. Bourilkov, L. Cadamuro, V. Cherepanov, F. Errico, R.D. Field, D. Guerrero, B.M. Joshi, M. Kim, J. Konigsberg, A. Korytov, K.H. Lo, K. Matchev, N. Menendez, G. Mitselmakher, D. Rosenzweig, K. Shi, J. Wang, S. Wang, X. Zuo

Florida International University, Miami, USA

Y.R. Joshi

Florida State University, Tallahassee, USA

T. Adams, A. Askew, D. Diaz, R. Habibullah, S. Hagopian, V. Hagopian, K.F. Johnson, R. Khurana, T. Kolberg, G. Martinez, T. Perry, H. Prosper, C. Schiber, R. Yohay, J. Zhang

Florida Institute of Technology, Melbourne, USA

M.M. Baarmann, M. Hohlmann, D. Noonan, M. Rahmani, M. Saunders, F. Yumiceva

University of Illinois at Chicago (UIC), Chicago, USA

M.R. Adams, L. Apanasevich, R.R. Betts, R. Cavanaugh, X. Chen, S. Dittmer, O. Evdokimov, C.E. Gerber, D.A. Hangal, D.J. Hofman, V. Kumar, C. Mills, G. Oh, T. Roy, M.B. Tonjes, N. Varelas, J. Viinikainen, H. Wang, X. Wang, Z. Wu

The University of Iowa, Iowa City, USA

M. Alhusseini, B. Bilki⁵⁴, K. Dilsiz⁷³, S. Durgut, R.P. Gundrajula, M. Haytmyradov, V. Khristenko, O.K. Köseyan, J.-P. Merlo, A. Mestvirishvili⁷⁴, A. Moeller, J. Nachtman, H. Ogul⁷⁵, Y. Onel, F. Ozok⁷⁶, A. Penzo, C. Snyder, E. Tiras, J. Wetzel, K. Yi⁷⁷

Johns Hopkins University, Baltimore, USA

B. Blumenfeld, A. Cocoros, N. Eminizer, A.V. Gritsan, W.T. Hung, S. Kyriacou, P. Maksimovic, C. Mantilla, J. Roskes, M. Swartz, T.Á. Vámi

The University of Kansas, Lawrence, USA

C. Baldenegro Barrera, P. Baringer, A. Bean, S. Boren, A. Bylinkin, T. Isidori, S. Khalil, J. King, G. Krintiras, A. Kropivnitskaya, C. Lindsey, W. Mcbrayer, N. Minafra, M. Murray, C. Rogan, C. Royon, S. Sanders, E. Schmitz, J.D. Tapia Takaki, Q. Wang, J. Williams, G. Wilson

Kansas State University, Manhattan, USA

S. Duric, A. Ivanov, K. Kaadze, D. Kim, Y. Maravin, D.R. Mendis, T. Mitchell, A. Modak, A. Mohammadi

Lawrence Livermore National Laboratory, Livermore, USA

F. Rebassoo, D. Wright

University of Maryland, College Park, USA

E. Adams, A. Baden, O. Baron, A. Belloni, S.C. Eno, Y. Feng, N.J. Hadley, S. Jabeen, G.Y. Jeng, R.G. Kellogg, A.C. Mignerey, S. Nabili, M. Seidel, A. Skuja, S.C. Tonwar, L. Wang, K. Wong

Massachusetts Institute of Technology, Cambridge, USA

D. Abercrombie, B. Allen, R. Bi, S. Brandt, W. Busza, I.A. Cali, M. D'Alfonso, G. Gomez Ceballos, M. Goncharov, P. Harris, D. Hsu, M. Hu, M. Klute, D. Kovalevskyi, Y.-J. Lee, P.D. Luckey, B. Maier, A.C. Marini, C. Mcginn, C. Mironov, S. Narayanan, X. Niu, C. Paus, D. Rankin, C. Roland, G. Roland, Z. Shi, G.S.F. Stephans, K. Sumorok, K. Tatar, D. Velicanu, J. Wang, T.W. Wang, B. Wyslouch

University of Minnesota, Minneapolis, USA

R.M. Chatterjee, A. Evans, S. Guts[†], P. Hansen, J. Hiltbrand, Sh. Jain, Y. Kubota, Z. Lesko, J. Mans, M. Revering, R. Rusack, R. Saradhy, N. Schroeder, N. Strobbe, M.A. Wadud

University of Mississippi, Oxford, USA

J.G. Acosta, S. Oliveros

University of Nebraska-Lincoln, Lincoln, USA

K. Bloom, S. Chauhan, D.R. Claes, C. Fangmeier, L. Finco, F. Golf, R. Kamalieddin, I. Kravchenko, J.E. Siado, G.R. Snow[†], B. Stieger, W. Tabb

State University of New York at Buffalo, Buffalo, USA

G. Agarwal, C. Harrington, I. Iashvili, A. Kharchilava, C. McLean, D. Nguyen, A. Parker, J. Pekkanen, S. Rappoccio, B. Roozbahani

Northeastern University, Boston, USA

G. Alverson, E. Barberis, C. Freer, Y. Haddad, A. Hortiangtham, G. Madigan, B. Marzocchi, D.M. Morse, V. Nguyen, T. Orimoto, L. Skinnari, A. Tishelman-Charny, T. Wamorkar, B. Wang, A. Wisecarver, D. Wood

Northwestern University, Evanston, USA

S. Bhattacharya, J. Bueghly, G. Fedi, A. Gilbert, T. Gunter, K.A. Hahn, N. Odell, M.H. Schmitt, K. Sung, M. Velasco

University of Notre Dame, Notre Dame, USA

R. Bucci, N. Dev, R. Goldouzian, M. Hildreth, K. Hurtado Anampa, C. Jessop, D.J. Karmgard, K. Lannon, W. Li, N. Loukas, N. Marinelli, I. Mcalister, F. Meng, Y. Musienko³⁵, R. Ruchti, P. Siddireddy, G. Smith, S. Taroni, M. Wayne, A. Wightman, M. Wolf

The Ohio State University, Columbus, USA

J. Alimena, B. Bylsma, B. Cardwell, L.S. Durkin, B. Francis, C. Hill, W. Ji, A. Lefeld, B.L. Winer, B.R. Yates

Princeton University, Princeton, USA

G. Dezoort, P. Elmer, J. Hardenbrook, N. Haubrich, S. Higginbotham, A. Kalogeropoulos, G. Kopp, S. Kwan, D. Lange, M.T. Lucchini, J. Luo, D. Marlow, K. Mei, I. Ojalvo, J. Olsen, C. Palmer, P. Piroué, D. Stickland, C. Tully

University of Puerto Rico, Mayaguez, USA

S. Malik, S. Norberg

Purdue University, West Lafayette, USA

V.E. Barnes, R. Chawla, S. Das, L. Gutay, M. Jones, A.W. Jung, B. Mahakud, D.H. Miller, G. Negro, N. Neumeister, C.C. Peng, S. Piperov, H. Qiu, J.F. Schulte, N. Trevisani, F. Wang, R. Xiao, W. Xie

Purdue University Northwest, Hammond, USA

T. Cheng, J. Dolen, N. Parashar

Rice University, Houston, USA

A. Baty, U. Behrens, S. Dildick, K.M. Ecklund, S. Freed, F.J.M. Geurts, M. Kilpatrick, A. Kumar, W. Li, B.P. Padley, R. Redjimi, J. Roberts[†], J. Rorie, W. Shi, A.G. Stahl Leiton, Z. Tu, A. Zhang

University of Rochester, Rochester, USA

A. Bodek, P. de Barbaro, R. Demina, J.L. Dulemba, C. Fallon, T. Ferbel, M. Galanti, A. Garcia-Bellido, O. Hindrichs, A. Khukhunaishvili, E. Ranken, R. Taus

Rutgers, The State University of New Jersey, Piscataway, USA

B. Chiarito, J.P. Chou, A. Gandrakota, Y. Gershtein, E. Halkiadakis, A. Hart, M. Heindl, E. Hughes, S. Kaplan, I. Laflotte, A. Lath, R. Montalvo, K. Nash, M. Osherson, S. Salur, S. Schnetzer, S. Somalwar, R. Stone, S. Thomas

University of Tennessee, Knoxville, USA

H. Acharya, A.G. Delannoy, S. Spanier

Texas A&M University, College Station, USA

O. Bouhali⁷⁸, M. Dalchenko, A. Delgado, R. Eusebi, J. Gilmore, T. Huang, T. Kamon⁷⁹, H. Kim, S. Luo, S. Malhotra, D. Marley, R. Mueller, D. Overton, L. Perniè, D. Rathjens, A. Safonov

Texas Tech University, Lubbock, USA

N. Akchurin, J. Damgov, V. Hegde, S. Kunori, K. Lamichhane, S.W. Lee, T. Mengke, S. Muthumuni, T. Peltola, S. Undleeb, I. Volobouev, Z. Wang, A. Whitbeck

Vanderbilt University, Nashville, USA

S. Greene, A. Gurrola, R. Janjam, W. Johns, C. Maguire, A. Melo, H. Ni, K. Padeken, F. Romeo, P. Sheldon, S. Tuo, J. Velkovska, M. Verweij

University of Virginia, Charlottesville, USA

L. Ang, M.W. Arenton, P. Barria, B. Cox, G. Cummings, J. Hakala, R. Hirosky, M. Joyce, A. Ledovskoy, C. Neu, B. Tannenwald, Y. Wang, E. Wolfe, F. Xia

Wayne State University, Detroit, USA

R. Harr, P.E. Karchin, N. Poudyal, J. Sturdy, P. Thapa

University of Wisconsin - Madison, Madison, WI, USA

K. Black, T. Bose, J. Buchanan, C. Caillol, D. Carlsmith, S. Dasu, I. De Bruyn, L. Dodd, C. Galloni, H. He, M. Herndon, A. Hervé, U. Hussain, A. Lanaro, A. Loeliger, R. Loveless, J. Madhusudanan Sreekala, A. Mallampalli, D. Pinna, T. Ruggles, A. Savin, V. Sharma, W.H. Smith, D. Teague, S. Trembath-reichert, W. Vetens

[†]: Deceased

1: Also at Vienna University of Technology, Vienna, Austria

2: Also at Université Libre de Bruxelles, Bruxelles, Belgium

3: Also at IRFU, CEA, Université Paris-Saclay, Gif-sur-Yvette, France

4: Also at Universidade Estadual de Campinas, Campinas, Brazil

5: Also at Federal University of Rio Grande do Sul, Porto Alegre, Brazil

- 6: Also at UFMS, Nova Andradina, Brazil
- 7: Also at Universidade Federal de Pelotas, Pelotas, Brazil
- 8: Also at University of Chinese Academy of Sciences, Beijing, China
- 9: Also at Institute for Theoretical and Experimental Physics named by A.I. Alikhanov of NRC 'Kurchatov Institute', Moscow, Russia
- 10: Also at Joint Institute for Nuclear Research, Dubna, Russia
- 11: Also at Zewail City of Science and Technology, Zewail, Egypt
- 12: Also at Purdue University, West Lafayette, USA
- 13: Also at Université de Haute Alsace, Mulhouse, France
- 14: Also at Erzincan Binali Yildirim University, Erzincan, Turkey
- 15: Also at CERN, European Organization for Nuclear Research, Geneva, Switzerland
- 16: Also at RWTH Aachen University, III. Physikalisches Institut A, Aachen, Germany
- 17: Also at University of Hamburg, Hamburg, Germany
- 18: Also at Brandenburg University of Technology, Cottbus, Germany
- 19: Also at Institute of Physics, University of Debrecen, Debrecen, Hungary, Debrecen, Hungary
- 20: Also at Institute of Nuclear Research ATOMKI, Debrecen, Hungary
- 21: Also at MTA-ELTE Lendület CMS Particle and Nuclear Physics Group, Eötvös Loránd University, Budapest, Hungary, Budapest, Hungary
- 22: Also at IIT Bhubaneswar, Bhubaneswar, India, Bhubaneswar, India
- 23: Also at Institute of Physics, Bhubaneswar, India
- 24: Also at G.H.G. Khalsa College, Punjab, India
- 25: Also at Shoolini University, Solan, India
- 26: Also at University of Hyderabad, Hyderabad, India
- 27: Also at University of Visva-Bharati, Santiniketan, India
- 28: Now at INFN Sezione di Bari ^a, Università di Bari ^b, Politecnico di Bari ^c, Bari, Italy
- 29: Also at Italian National Agency for New Technologies, Energy and Sustainable Economic Development, Bologna, Italy
- 30: Also at Centro Siciliano di Fisica Nucleare e di Struttura Della Materia, Catania, Italy
- 31: Also at Riga Technical University, Riga, Latvia, Riga, Latvia
- 32: Also at Malaysian Nuclear Agency, MOSTI, Kajang, Malaysia
- 33: Also at Consejo Nacional de Ciencia y Tecnología, Mexico City, Mexico
- 34: Also at Warsaw University of Technology, Institute of Electronic Systems, Warsaw, Poland
- 35: Also at Institute for Nuclear Research, Moscow, Russia
- 36: Now at National Research Nuclear University 'Moscow Engineering Physics Institute' (MEPhI), Moscow, Russia
- 37: Also at Institute of Nuclear Physics of the Uzbekistan Academy of Sciences, Tashkent, Uzbekistan
- 38: Also at St. Petersburg State Polytechnical University, St. Petersburg, Russia
- 39: Also at University of Florida, Gainesville, USA
- 40: Also at Imperial College, London, United Kingdom
- 41: Also at P.N. Lebedev Physical Institute, Moscow, Russia
- 42: Also at California Institute of Technology, Pasadena, USA
- 43: Also at Budker Institute of Nuclear Physics, Novosibirsk, Russia
- 44: Also at Faculty of Physics, University of Belgrade, Belgrade, Serbia
- 45: Also at Università degli Studi di Siena, Siena, Italy
- 46: Also at INFN Sezione di Pavia ^a, Università di Pavia ^b, Pavia, Italy, Pavia, Italy
- 47: Also at National and Kapodistrian University of Athens, Athens, Greece
- 48: Also at Universität Zürich, Zurich, Switzerland

-
- 49: Also at Stefan Meyer Institute for Subatomic Physics, Vienna, Austria, Vienna, Austria
50: Also at Burdur Mehmet Akif Ersoy University, BURDUR, Turkey
51: Also at Şırnak University, Sirnak, Turkey
52: Also at Department of Physics, Tsinghua University, Beijing, China, Beijing, China
53: Also at Near East University, Research Center of Experimental Health Science, Nicosia, Turkey
54: Also at Beykent University, Istanbul, Turkey, Istanbul, Turkey
55: Also at Istanbul Aydin University, Application and Research Center for Advanced Studies (App. & Res. Cent. for Advanced Studies), Istanbul, Turkey
56: Also at Mersin University, Mersin, Turkey
57: Also at Piri Reis University, Istanbul, Turkey
58: Also at Ozyegin University, Istanbul, Turkey
59: Also at Izmir Institute of Technology, Izmir, Turkey
60: Also at Bozok Universitetesi Rektörlüğü, Yozgat, Turkey
61: Also at Marmara University, Istanbul, Turkey
62: Also at Milli Savunma University, Istanbul, Turkey
63: Also at Kafkas University, Kars, Turkey
64: Also at Istanbul Bilgi University, Istanbul, Turkey
65: Also at Hacettepe University, Ankara, Turkey
66: Also at Adiyaman University, Adiyaman, Turkey
67: Also at Vrije Universiteit Brussel, Brussel, Belgium
68: Also at School of Physics and Astronomy, University of Southampton, Southampton, United Kingdom
69: Also at IPPP Durham University, Durham, United Kingdom
70: Also at Monash University, Faculty of Science, Clayton, Australia
71: Also at Bethel University, St. Paul, Minneapolis, USA, St. Paul, USA
72: Also at Karamanoğlu Mehmetbey University, Karaman, Turkey
73: Also at Bingol University, Bingol, Turkey
74: Also at Georgian Technical University, Tbilisi, Georgia
75: Also at Sinop University, Sinop, Turkey
76: Also at Mimar Sinan University, Istanbul, Istanbul, Turkey
77: Also at Nanjing Normal University Department of Physics, Nanjing, China
78: Also at Texas A&M University at Qatar, Doha, Qatar
79: Also at Kyungpook National University, Daegu, Korea, Daegu, Korea